Published OnlineFirst December 18, 2019; DOI: 10.1158/2326-6066.CIR-19-0493

CD40 Enhances Type I Interferon Responses Downstream of CD47 Blockade, Bridging Innate and Adaptive Immunity

Suresh de Silva, George Fromm, Casey W. Shuptrine, Kellsey Johannes, Arpita Patel, Kyung Jin Yoo, Kaiwen Huang, and Taylor H. Schreiber

ABSTRACT

Disrupting the binding of CD47 to SIRPα has emerged as a promising immunotherapeutic strategy for advanced cancers by potentiating antibody-dependent cellular phagocytosis (ADCP) of targeted antibodies. Preclinically, CD47/SIRPα blockade induces antitumor activity by increasing the phagocytosis of tumor cells by macrophages and enhancing the cross-presentation of tumor antigens to $CD8^+$ T cells by dendritic cells; both of these processes are potentiated by CD40 signaling. Here we generated a novel, two-sided fusion protein incorporating the extracellular domains of SIRPα and CD40L, adjoined by a central Fc domain, termed SIRPα-Fc-CD40L. SIRPα-Fc-CD40L bound CD47 and CD40 with high affinity and activated CD40 signaling in the absence of Fc receptor cross-linking. No evidence of hemolysis, hemagglutination, or thrombocytopenia was observed *in vitro* or in cynomolgus macaques. Murine SIRPα-Fc-CD40L outperformed CD47 blocking and CD40 agonist antibodies in murine CT26 tumor models and synergized with immune checkpoint blockade of PD-1 and CTLA4. SIRPα-Fc-CD40L activated a type I interferon response in macrophages and potentiated the activity of ADCP-competent targeted antibodies both *in vitro* and *in vivo*. These data illustrated that whereas CD47/SIRPα inhibition could potentiate tumor cell phagocytosis, CD40-mediated activation of a type I interferon response provided a bridge between macrophage- and T-cell–mediated immunity that significantly enhanced durable tumor control and rejection.

Introduction

Tumor immunogenicity results from the processing, and subsequent presentation of tumor antigens released from dead or dying tumor cells on MHC molecules expressed on antigen-presenting cells (APC). The CD47/SIRPα pathway is an endogenous pathway that facilitates clearance of aged or dying cells (1). CD47 is expressed by many somatic and hematopoietic tissues and prevents red blood cell (RBC) and platelet destruction by macrophages and splenic $CD4^+$ dendritic cells (DC; refs. 2–6). The antiphagocytic activity of CD47/SIRPα serves as a macrophage checkpoint or "do not eat me" signal (1). The prophagocytic "eat me" signal that triggers RBC destruction by splenic macrophages is dependent upon a second "activating" signal, which includes CD18-containing integrins and "labeling" of susceptible cells by calreticulin (5, 7).

Many tumors have increased expression of CD47 suggesting a coopted protective mechanism against immune-mediated destruction. Early studies hypothesized that the role of CD47 as a macrophage "do not eat me" signal might explain the observed antitumor benefit following treatment with CD47 blocking antibodies or SIRPα-Fc fusion proteins (8–10). Other studies extended these observations to show that SIRPα signaling in $CD8\alpha^+$ DCs enhances cGAS/STING-mediated sensing of phagocytosed tumor mitochondrial DNA, promoting a type I IFN response that facilitates cross-presentation of tumor antigens to $CD8^+$ T cells (11, 12). Increased priming of $CD8^+$ T cells in the presence of CD47/SIRPα inhibition dramatically enhanced tumor rejection in multiple preclinical tumor models (11, 12), demonstrating that the CD47/SIRPα axis is capable of bridging innate and adaptive immunity.

$CD8\alpha^+$ DCs expressing the transcription factor BATF3 are essential for antitumor immunity (13) and have the unique ability to cross-present exogenous tumor antigens, which gain entry to the cytosol of DCs following endocytosis, to $CD8^+$ T cells. CD40 ligation by CD40 ligand (CD40L), expressed by resting $CD8\alpha^+$ (but not $CD8\alpha^-$) DCs, enhances the antigen cross-presenting activity of DCs (14–18). Interestingly, whereas CD40 ligation facilitates a type I IFN response via STING activation, STING activation is not essential for the antitumor immune response to CD40 stimulation (19, 20). However, antitumor immunity to CD40 agonists is dependent on $BATF3^+$ DCs and $CD8^+$ T cells (19). These data indicate that, like CD47/SIRPα, the CD40/CD40L axis is capable of bridging innate and adaptive immunity; however, the two pathways appear to have distinct dependence upon a type I IFN response.

The nonoverlapping roles of CD47/SIRPα and CD40/CD40L in bridging innate and adaptive cancer immunotherapy suggests that these two pathways could be complimentary or synergistic in combination. SIRPα-Fc fusion proteins, CD40L-Fc fusion proteins, and CD40 agonist antibodies have been successfully used as therapeutics (21–28). The extracellular domains (ECD) of PD-1 and OX40L can be adjoined via an Fc domain (PD-1-Fc-OX40L), leading to superior therapeutic properties compared with anti-PD-1 and anti-OX40 combinations (29). As a result, we sought to develop a SIRPα-Fc-CD40L agonist redirected checkpoint (ARC) fusion protein to approach these distinct pathways with a single biologic. Given the costimulatory role of CD40 in augmenting the antigen cross-presenting ability of DCs and also the phagocytic activity of macrophages, we hypothesized that pairing SIRPα with CD40L may enhance antitumor immunity (30).

Shattuck Labs, Inc., Durham, North Carolina.

Note: Supplementary data for this article are available at Cancer Immunology Research Online (http://cancerimmunolres.aacrjournals.org/).

S. de Silva and G. Fromm contributed equally to this article.

Corresponding Author: Taylor H. Schreiber, Shattuck Labs, Inc., 21 Parmer Way, Suite 200, Durham, NC 27709. Phone: 919-864-2700; E-mail: tschreiber@shattucklabs.com

Cancer Immunol Res 2020;8:230–45

doi: 10.1158/2326-6066.CIR-19-0493

Here, we developed and characterized a SIRPα-Fc-CD40L for both humans and mice. Human SIRPα-Fc-CD40L engaged CD47 and CD40 simultaneously and with high affinity, causing activation of primary human T cells *in vitro* by increasing cytokine production, proliferation, and activation of NFκB and NIK signaling. In mouse models, murine SIRPα-Fc-CD40L provided higher rates of tumor rejection and long-term immunity compared with CD47 blocking antibodies, CD40 agonist antibodies, or the combination of the two. The mechanism of action of SIRPα-Fc-CD40L was attributed to enhanced activation of DCs *in vivo*, upregulation of a type I IFN response, and potentiation of macrophage-mediated phagocytosis *in vitro*. Taken together, CD40 synergistically enhanced the antitumor activity of CD47/SIRPα blockade by upregulating the type I IFN response in macrophages.

Materials and Methods

Construct generation and protein purification

The coding sequences of both human (h) and mouse (m) SIRPα-Fc-CD40L were codon-optimized and directionally cloned into the pcDNA3.4 TOPO TA (Thermo Fisher Scientific, catalog no. A14697; Supplementary Table S1) mammalian expression vector and nucleotide sequences were verified by Sanger sequencing methodology (performed off site by GENEWIZ). For transient transfection–based protein production runs, human or mouse SIRPα-Fc-CD40L–expressing vectors were transfected into Expi293 cells using the ExpiFectamine 293 transfection kit (Thermo Fisher Scientific, catalog no. A14524) and cell culture media containing SIRPα-Fc-CD40L was harvested on day 6 posttransfection. In addition, the hSIRPα-Fc-CD40L vector was stably transfected into CHO cells and a final clone expressing high levels of hSIRPα-Fc-CD40L was selected for large scale protein production and purification (Selexis SA). Briefly, SIRPα-Fc-CD40L containing cell culture media was harvested by centrifugation at 5,000 rpm for 10 minutes followed by filtration through a 0.2-μm filter. The clarified supernatant was bound to a HighTrap Protein A HP column, washed and eluted under standard conditions. The eluted protein was dialyzed into 1× PBS and the concentration was determined by absorption at 280 nm using a NanoDrop spectrophotometer (Thermo Fisher Scientific).

Western blot analysis

Human (h) and mouse (m) SIRPα-Fc-CD40L proteins were treated with or without the deglycosylase PNGase F (NEB, catalog no. P0704) for 1 hour at 37°C according to manufacturer's recommendations, and then with or without the reducing agent β-mercaptoethanol, and diluted in SDS loading buffer prior to separation by SDS-PAGE. Primary and secondary antibodies were used for probing hSIRPα-Fc-CD40L (anti-SIRPα; Cell Signaling Technology, catalog no. 43248S, anti-human IgG; Jackson ImmunoResearch, catalog no. 109-005-098, anti-CD40L; R&D Systems, catalog no. AF1054), and mSIRPα-Fc-CD40L (anti-SIRPα; BioLegend, catalog no. 144001, anti-mouse IgG; Jackson ImmunoResearch, catalog no. 115-005-068, anti-CD40L; R&D Systems, catalog no. AF1163). Secondary anti-goat IgG and anti-rabbit IgG were obtained from LI-COR; catalog numbers 925-32214 and 925-32211, respectively.

Electron microscopy

Samples were diluted in PBS (30- to 140-fold) and imaged over a layer of continuous carbon supported by nitrocellulose on a 400-mesh copper grid. Electron microscopy was performed using an FEI Tecnai T12 electron microscope operating at 120 keV equipped with an FEI Eagle 4k × 4k CCD camera (NanoImaging Services). Negative stain grids were transferred into the electron microscope using a room temperature stage. Images of each grid were acquired at multiple scales to assess the overall distribution of the specimen. After identifying suitable target areas for imaging, high magnification images were acquired at nominal magnifications of 110,000× and 67,000×. The images were acquired at a nominal underfocus of −1.6 μmol/L to −0.9 μmol/L and electron doses of approximately 25 e^{-}/A^{2}. Two-dimensional averaging analysis was performed using automated picking protocols followed by reference-free alignment based on the XMIPP processing package (31, 32).

Functional ELISA

For characterization of the h/m SIRPα-Fc-CD40L ARCs, high-binding ELISA plates (Corning) were coated overnight at 4°C with 5 μg/mL of either anti-hFc, anti-mFc, recombinant hCD47-Fc, hCD40-His, mCD47-Fc or mCD40-His, in PBS (reagents were obtained from Jackson ImmunoResearch Laboratories, Sino Biologics, Inc., Acro-Biosystems, and R&D Systems). Plates were then blocked with casein buffer for 1 hour at room temperature and then probed with serial dilutions of the h/m SIRPα-Fc-CD40L, along with the appropriate standards (human and mouse; IgG, SIRPα-Fc, and Fc-CD40L) for 1 hour at room temperature. Plates were washed with TBS-T (Tris-buffered saline containing 0.1% Tween 20) and then detection antibody was added for 1 hour at room temperature in the dark. Detection antibodies included anti-hIgG-HRP, anti-mIgG-HRP, anti-hCD40L, anti-mCD40L, and then anti-Goat-HRP (all antibodies were obtained from Jackson ImmunoResearch Laboratories or R&D Systems). Plates were washed again and SureBlue TMB Microwell Peroxidase Substrate (KPL; purchased from VWR, catalog no. 95059-282) was added to each well and allowed to incubate at room temperature in the dark. To stop the reaction, 1N sulfuric acid was added to each well and absorbance at 450 nm was read immediately on a BioTek plate reader. Samples were run at a minimum in triplicate and at multiple dilutions.

For SIRPα-blocking ELISA, hCD47-Fc (Sino Biological Inc.) was used to coat a high binding ELISA plate as described above. The following day, binding was detected using a recombinant hSIRPα-Biotin protein (Acro Biosystems) in combination with increasing concentrations of either hSIRPα-Fc-CD40L (to compete with SIRPα-Biotin binding for CD47) or an anti-CD47 blocking antibody (clone CC2C6, BioLegend), which served as a positive control. Following this incubation, plates were washed as described above and probed with an avidin–HRP detection antibody (BioLegend) for 1 hour at room temperature in the dark. Plates were then washed and analyzed as above.

Surface plasmon resonance

Direct binding of h/m SIRPα-Fc-CD40L fusion protein to recombinant protein targets was performed using a Bio-Rad ProteOn XPR36 protein interaction array instrument. To determine the on-rates (K_a), off-rates (K_d), and binding affinities (KD) of hSIRPα-Fc-CD40L to its intended binding targets (referred to as "Ligands"), histidine-tagged versions of the human recombinant targets–CD47 (AcroBiosystems), CD40 (AcroBiosystems), FcγR1A (Sino Biological Inc.), FcγR2B (Sino Biological Inc.), FcγR3B (Sino Biological Inc.), and FcRn (R&D Systems) were immobilized to a Ni-sulfate activated ProteOn HTG sensor chip (Bio-Rad). Increasing concentrations of the hSIRPα-Fc-CD40L fusion protein (referred to as "Analyte") diluted in PBS/Tween (0.005%) buffer pH 7.0 were injected for 3 minutes followed by a dissociation phase of 5 minutes at a flow rate of 80 μL/minute. hSIRPα-Fc and hCD40L-Fc (AcroBiosystems) recombinant proteins were used

Published OnlineFirst December 18, 2019; DOI: 10.1158/2326-6066.CIR-19-0493

as positive control analytes for binding to their partners (CD47 and CD40, respectively) and human IgG was used as a positive control for binding to Fcγ receptors and FcRn. To assess analyte binding to FcRn ligand, the pH of the buffer was reduced to pH 5.5.

Cell culture

CHO-K1, CT26, A20, WEHI3, Toledo, Raji, Ramos, A431, HCC827, K562, HCC1954, and MCF7 cells were obtained from ATCC (between 2017 and 2019) and cultured according to their guidelines; maintained at 37°C in 5% CO_2. All parental cell lines in active culture are tested monthly using the Venor GeM Mycoplasma Detection Kit (Sigma). All transfected cell lines are tested an additional two times, separated by at least 2 weeks, posttransfection, and confirmed to remain negative for *Mycoplasma*. Research cell banks (RCB) of all purchased cell lines were generated within 5 passages of initial cell line thawing. All cells used for experimentation were used within 10 passages of vial thawing. Expression from receptor/ligand over-expressing cells lines was verified by flow cytometry prior to generating the RCB, and then periodically checked again when new vials were thawed and put into culture.

In vitro cell line generation

Stable cells lines were generated to assess *in vitro* binding of human and mouse SIRPα-Fc-CD40L ARC proteins. To generate the CHO-K1/hCD47, CHO-K1/mCD47, and CHO-K1/mCD40 cell lines, total RNA was extracted from CD3/CD28 activated human PBMCs and mouse splenocytes (1×10^6 cells) using the RNeasy mini kit (Qiagen, catalog no.74104) and 1 μg of RNA was used to generate first strand cDNA using a commercial kit (Origene, catalog no. 11801-025). One microliter of the resulting first strand cDNA was used to PCR amplify each of the targets using Platinum Taq DNA polymerase (Thermo Fisher Scientific, catalog no. 10966034) and the following primer pairs with restriction enzyme sites appended to the 5′ ends for subcloning the PCR fragment into the pcDNA3.1(-) expression vector (Life Technologies) using standard molecular biology techniques- hCD47 forward 5′ GCGGCGCTCGAGGCCACCATGTGGCCCCTGGTAGCGG; hCD47 reverse 5′ ACTAGCGGTACCCCATCACTTCACTTCAGTTATTCCACAAATTTC; mCD47 forward 5′ GCGGCGCTCGAGGCCACCATGTGGCCCTTGGCGGC, mCD47 reverse 5′ ACTAGCGGTACCTCACCTATTCCTAGGAGGTTGGATAGTCC; mCD40 forward 5′ GCGGCGCTCGAGGCCACCATGGTGTCTTTGCCTCGGCTG; mCD47 reverse 5′ ACTAGCGGTACCTCAGACCAGGGGCCTCAAG. The CHOK1-hCD40 cell line was generated by cloning the hCD40 cDNA (R&D Systems #RD1325) into pcDNA3.1(-) vector. The nucleotide sequences of the subcloned cDNAs in the pcDNA3.1(-) vector were confirmed by sanger sequencing (GENEWIZ). Parental CHO-K1 cells were nucleofected with each of the target cDNA expressing pcDNA3.1(-) vectors using the 4D-Nucleofector and Cell Line Nucleofector Kit SE (Lonza, catalog no. V4XC-1012) according to manufacturer's directions. Two days postnucleofection the cells were placed under G418 selection (0.5 mg/mL) for two weeks and the stable pool was subsequently single-cell–cloned using limiting dilution to isolate clones that expressed high amounts of the target receptors, which was confirmed by flow cytometry using the following APC-conjugated fluorescent antibodies from BioLegend–anti-hCD40 (catalog no. 334310), anti-hCD47 (catalog no. 323124), anti-mouse CD40 (catalog no. 124612), and anti-mouse CD47 (catalog no. 127514). CHO-K1/mCD40 and CHO-K1/hCD40 cells were also subsequently stably nucloefected with pGL4.32[luc2P/NF-κB-RE/Hygro] (Promega) reporter plasmid, to generate CD40-driven NFκB reporter cells.

Flow cytometry

Briefly, isolated cells were washed one time with 1× PBS, followed by centrifugation at 400 × *g* for 5 minutes. Cells were then stained with antibodies for 30 minutes on ice in the dark. Indicated antibodies were purchased from Sony, BioLegend, or Abcam, and used at their recommended concentrations, and diluted in FACS buffer [1× PBS buffer containing 1% BSA, 0.02% sodium azide, and 2 mmol/L EDTA]. The AH1-tetramer reagent was purchased from MBL International (catalog no. TB-M521-2), and was incubated with cells for 1 hour on ice in the dark before adding the rest of the antibody cocktail. Following this incubation period, stained cells were washed by adding 0.5 mL of FACS buffer, and then centrifuged at 400 × *g* for 5 minutes. The supernatant above the pellet was then aspirated and the resulting cells were resuspended in FACS buffer and flow cytometry was performed on a BD LSRII Fortessa according to manufacturer's recommendations, and data were analyzed by FlowJo.

In vitro functional assays

Phagocytosis assay

Frozen vials of peripheral blood mononuclear cells (PBMC) from healthy human donors were purchased from STEMCELL Technologies and monocytes were isolated using a commercial kit according to the manufacturer's protocol (STEMCELL, catalog no. 19059) and were confirmed to be $CD14^+$ by flow cytometry postisolation using an APC-conjugated anti-human CD14 (BioLegend, catalog no. 367118) and the appropriate isotype control antibody. Following the isolation of monocytes, a live cell count was performed using Trypan blue staining 4×10^5 live and monocytes were seeded in Iscove modified Dulbecco media (IMDM) containing 10% FBS and 50 ng/mL of human macrophage colony-stimulating factor (M-CSF; BioLegend) in 24-well plates (Corning). Cells were incubated in 37°C/5% CO_2 for 7 days to differentiate into macrophages. Media were changed on day 4 and supplemented with M-CSF. On day 7, macrophages were polarized to an M1 state by replacing the media with fresh media containing 10 ng/mL lipopolysaccharide (LPS-EB; InvivoGen) and 50 ng/mL human IFNγ (STEMCELL Technologies). Cells were incubated for another 48 hours and M1 polarization status was confirmed by flow cytometry for CD11b, HLA-DR, CD80, and CD206 (BioLegend). Macrophages were confirmed to be M1 polarized if they stained positive for CD11b, HLA-DR, and CD80 and negative for CD206. On day 9, the media containing LPS and IFNγ was replaced with fresh media (IMDM + 10% FBS), and macrophage:tumor cocultures were initiated.

Flow cytometry–based analysis: Tumor cells were harvested and incubated with SIRPα-Fc-CD40L either alone at 1 μmol/L test concentration or in combination with select antibody-dependent cellular phagocytosis (ADCP)–competent antibodies (based on the type of tumor cell used in the assay) at 0.06 μmol/L test concentration for 37°C for 1 hour. Following the incubation, cells were washed with Dulbecco PBS (DPBS) and stained with a CellTracker Green CMFDA dye (Thermo Fisher Scientific/Invitrogen, catalog no. C2925) according to the manufacturer guidelines. Cells were washed twice with DPBS and resuspended in serum-free media. The stained tumor cells were cocultured with M1-polarized macrophages for 2 hours at 37°C at a tumor:macrophage ratio of 5:1. When appropriate, Fc receptors and CD40 receptors were blocked on macrophages using commercial antibodies (20 μg/mL; BioLegend and R&D Systems, respectively) and calreticulin was blocked on tumor cells using a calreticulin blocking peptide (10 μg/mL; MBL International Corporation) for 1 hour at 37°C prior to coculture initiation. After the coculture

incubation period, unbound/unengulfed tumor cells were removed and the macrophages were rinsed in DPBS and harvested using a nonenzymatic cell stripping solution (Thermo Fisher Scientific/Corning, catalog no. 25-056-C1). Harvested macrophage Fc receptors were blocked using a commercial human Fc blocking reagent (BioLegend). Thereafter, the Fc-receptor blocked macrophages were stained with an anti-human CD11b antibody conjugated to PE/Cy7 (BioLegend), washed, and analyzed on an LSRII Fortessa flow cytometer (BD Biosciences) to detect macrophages that stained positive for both CD11b and the CellTracker Green CMFDA dye following a phagocytic event. Cells were pregated on $CD11b^+$ macrophages. Samples were analyzed on a LSRII Fortessa and flow cytometry standard (FCS) files were analyzed using the FlowJo software version 10. The percentage of $CD11b^+$ Green dye^+ macrophages were plotted in GraphPad Prism 8. A phagocytosis index was calculated by setting the maximum response across the treatment groups to 1 and calculating the fold change for each of the treatment groups relative to the maximum response. A similar flow-based methodology was used to study phagocytosis of mouse tumor cells (WEHI or A20) by bone marrow–derived macrophages (BMDM) with mouse SIRPα-Fc-CD40L or mouse anti-CD47 (BioXCell, clone MIAP301). BMDMs were isolated and grown in IMDM with 10% FBS supplemented with mouse M-CSF (50 ng/mL) for 7 days, and activated with LPS (10 ng/mL) and mIFNγ (50 ng/mL) for 2 days.

Fluorescence microscopy–based analysis: Human monocytes ($CD14^+$) were plated in 16-well chamber glass slides (Thermo Fisher Scientific) to differentiate into macrophages and were polarized to an M1 state using LPS and IFNγ as described above. On the day of the experiment, tumor cells (Toledo) were prepared and cocultured with the M1 macrophages in the chamber slides in the presence of SIRPα-Fc-CD40L either alone or in combination with select ADCP-competent antibodies for 2 hours at 37°C. After the incubation period the unbound/unengulfed tumor cells were removed from the wells and the macrophages were rinsed four times in 1× DPBS. Subsequent blocking and staining steps were performed in the chamber slide. The Fc receptors on macrophages were blocked as described previously and subsequently stained with an anti-human CD11b antibody conjugated to Alexa Fluor 594 (BioLegend) overnight at 4°C protected from light. Macrophages were rinsed twice in DPBS to remove unbound stain and coverslips were mounted in ProLong Diamond anti-fade mountant containing DAPI (Invitrogen) and allowed to dry overnight at room temperature protected from light. Once dry, the edges of the coverslips were sealed with clear nail polish and fluorescent imaging was performed on a Zeiss 800 confocal microscope. Four representative images were acquired per well in the chamber slide under 10× and 60× magnifications and ImageJ software (NIH, Bethesda, MD) was used to process the raw images and quantify the number of engulfed tumor cells (labeled green) per total macrophages (labeled red) based on the pixel density. The compiled data included one representative image per condition and the quantification data incorporated at least four images per well and two wells per condition.

Time-lapse microscopy-based analysis: Human monocytes ($CD14^+$) were plated in a 96-well plate (Millipore Sigma), differentiated into macrophages, and polarized to an M1 state using LPS and IFNγ as described above. On the day of the experiment, Toledo tumor cells were labeled with the IncuCyte phRodo Red cell labeling kit (Sartorius, catalog no. 4649) according to the manufacturer's guidelines and then were cocultured with the M1 macrophages at a 5:1 ratio in the presence of SIRPα-Fc-CD40L (1 μmol/L), anti-CD20 (rituximab; 1 μg/mL), anti-CD47 (BioLegend clone CC2C6; 33 μg/mL); or the combination of anti-CD20 with either SIRPα-Fc-CD40L or anti-CD47. The 96-well plate was placed in the IncuyCyte S3 and time-lapse imaging was performed over the course of 5 hours at 37°C. Five images per well, in duplicate, using two distinct donors were acquired under 10× magnification for each treatment group and the red object integrated intensity per image was calculated using the IncuCyte S3 software. The phagocytosis index was calculated by taking the maximum signal observed from each experiment and setting that as the 100% point. Each data point from a given experiment was normalized to the maximum value for that experiment (i.e., fluorescence or luminescence). These calculations were repeated for each experimental replicate, and then all combined data was plotted using GraphPad Prism 8.

In vivo DC activation assay

BALB/C mice were obtained from Jackson Laboratories, and treated with a single intravenous injection of 1×10^7 PBS washed sheep red blood cells (RBC diluted in PBS; Rockland Immunochemicals), anti-CD47 (clone MIAP301), anti-SIRPα (clone P84), or mSIRPα-Fc-CD40L. Antibodies were given at a total dose of 100 μg and the ARC at 300 μg; all in a volume of 100 μL diluted in PBS. After 6 or 24 hours, mice were humanely euthanized and splenocytes were isolated for flow cytometry–based immune profiling of DCs, by removing the spleens from treated animals, mechanically dissociating them using the flat ends of two razors followed by repeated pipetting to break up larger pieces, and then passing the cells through a 100-μm cell strainer. RBCs were lysed with RBC lysis buffer according to manufacturer's recommendations (BioLegend, catalog no. 420301) and the remaining mononuclear cells were stained with fluorescent-conjugated antibodies to CD11c, DC1R2, $I\text{-}A^b$ (MHC-II), and either CD4 or CD8. After 30 minutes on ice in the dark, cells were washed, and then analyzed on an LSR II Fortessa flow cytometer. $CD4^+$ or $CD8^+$ DCs were pregated on $CD11c^+/DC1R2^+$ populations, and activated DCs were also positive for $I\text{-}A^b$. Additional pharmacodynamic activity was assessed in the peripheral blood, 24 hours following single intraperitoneal injections of a dose titration of mSIRPα-Fc-CD40L. A small amount of peripheral blood was collected from the tail and RBCs were lysed as described above. Populations of $CD20^+$ cells were assessed by flow cytometry.

NFκB-Luciferase reporter assay

CHOK1/mCD40/NFκB-luciferase cells were treated with a dose titration of mSIRPα-Fc-CD40L, recombinant Fc-mCD40L protein (Sino Biologics), or anti-mCD40 (clone FGK4.5; BioXcell). CHOK1/hCD40/NFκB-luciferase cells, were treated with a dose titration of SIRPα-Fc-CD40L and recombinant hCD40L-His protein (Sino Biologics). Bright-Glo luciferase reagent and a GloMax Navigator luminometer were used to assess activation of NFκB signaling. The expression vector, luciferase reagent (catalog no. E2650), and luminometer (catalog no. GM2000) are all from Promega and were used according to manufacturer suggestions. Briefly, 10,000 CHO-K1/CD40/NFκB-luciferase cells were plated in each well of a 96-well plate ± the ARC or other test agents. Plates were incubated at 37°C/5% CO_2 for 6 hours, then the Bright-Glo reagent was added and luminescence was assessed on the luminometer.

NIK/NFκB reporter assay

U2OS/NIK/NFκB reporter cells expressing CD40 were purchased from Eurofins/DiscoverX (catalog no. 93-1059C3) and cultured according to their recommendations. On the day of the assay,

Published OnlineFirst December 18, 2019; DOI: 10.1158/2326-6066.CIR-19-0493

10,000 U2OS/NIK/NFκB reporter cells were plated into each well of a 96-well plate with a dose titration of either SIRPα-Fc-CD40L, recombinant Fc-hCD40L protein (Sino Biologics), or an anti-CD40 agonist antibody (clone HB14; BioLegend). After 6 hours in culture, luminescence activity was assessed on a luminometer (Promega) as described above.

AIMV activation assay

Proliferation: PBMCs were isolated from 50 healthy donor buffy coats and $CD8^+$ T cells were depleted using $CD8^+$ RosetteSep (STEMCELL Technologies). Cell depletion was confirmed by flow cytometry and was >90% for all donors. Cells were plated at a density of 4–6 million cells per mL in AIM-V medium (Gibco). On days 5, 6, and 7, cells were gently resuspended in 3 × 100 μL aliquots and transferred to each well of a round-bottom 96-well plate. Cultures were pulsed with 0.75 μCi [3H]-Thymidine (PerkinElmer) in 100 μL AIM-V culture medium, and incubated for a further 18 hours, before harvesting onto filter mats (PerkinElmer), using a TomTec Mach III cell harvester. Counts per minute (cpm) for each well were determined by Meltilex (PerkinElmer) scintillation counting on a 1450 Microbeta Wallac Trilux Liquid Scintillation Counter (PerkinElmer), with low background counting.

IL2 ELISpot: PBMCs were isolated, CD8 cells depleted, and cultured in AIM-V as described above, and on day 8, cells were assessed. Briefly, ELISpot plates (Millipore) were prewetted and coated overnight with 100 μL/well IL2 capture antibody (R&D Systems) in PBS. Cells were plated at a density of 4–6 million cells/mL in a volume of 100 μL per well, in sextuplicate. After 8 days, ELISpot plates were developed by sequential washing in dH_2O and PBS (×3), prior to the addition of 100 μL filtered biotinylated detection antibody (R&D Systems). Following incubation at 37°C for 1.5 hours, plates were further washed with PBS and 1% BSA, and incubated with 100 μL filtered streptavidin-AP (R&D Systems) for 1 hour; and then washed again. One-hundred microliters BCIP/NBT substrate (R&D Systems) was added to each well for 30 minutes at room temperature. Spot development was stopped by washing wells three times with dH_2O. Dried plates were scanned on an Immunoscan Analyzer and spots per well (SPW) were determined using Immunoscan Version 5 software. Samples included human SIRPα-Fc-CD40L (at 0.3, 3, 30, and 300 nmol/L), the neoantigen KLH (Keyhole limpet hemocyanin; 300 nmol/L) as a positive control, and exenatide (Bydureon, 20 μmol/L) as a clinical benchmark control; representing a negative control in this assay. For ELISpot, a mitogen-positive control (PHA at 8 μg/mL) was included on each plate as an internal test for ELISpot function and cell viability.

Type I IFN response

Gene expression analysis

Human macrophage:Toledo/Raji tumor cocultures were set up as described above. After 2 hours of coculture and treatment with either SIRPα-Fc-CD40L (1 μmol/L), anti-human CD20/rituximab (0.06 μmol/L), or the combination of both agents; cells were collected from the plate using a nonenzymatic cell stripping solution (Thermo Fisher Scientific/Corning, catalog no. 25-056-C1), washed with PBS, and stained with a fluorescently conjugated antibody for CD11b, after Fc blocking. After a 30-minute incubation on ice in the dark, cells were washed and $CD11b^+$ populations were sorted using a FACS Melody (BD Biosciences). Sorted macrophages were lysed with RLT lysis buffer (Qiagen RNeasy Micro Kit, catalog no. 74004) containing 5% 2-mercaptoethanol and processed according to manufacturer's directions; including on-column DNase I digestion. RNA was quantitated using a Nanodrop and 250 ng of resulting RNA was reverse transcribed (Origene First-strand cDNA Synthesis kit) according to manufacturer's recommendations. The resulting cDNA was diluted with nuclease-free water and the equivalent of 10 ng of starting RNA served as the template for each qPCR reaction. Gene expression was assessed using SYBR Green and the CFX96 Touch Real-Time PCR Detection System (Bio-Rad). Validated qPCR primers for IFNα1, IFNβ1, CD80, CD86 and β-Actin (ACTB) as a housekeeping control, were purchased from Origene. Fold change in gene expression was determined using the $\Delta\Delta C_t$ method compared with untreated samples. Data generated were from a minimum of three experimental replicates all run in at least triplicate. Error bars represent SEM and significance was determined using one-way ANOVA.

ISG reporter cells

RAW264.7-Lucia ISG cells were obtained from InvivoGen and cultured according to their recommendations. RAW-Lucia ISG cells were cultured directly with A20 tumor cells, and 50 μg/mL of mSIRPα-Fc-CD40L, recombinant mFc-CD40L, recombinant mSIRPα-Fc (both at 50 μg/mL), the combination of mFc-CD40L and mSIRPα-Fc, anti-mCD20 (BioXcell clone AISB12; 1 μg/mL), or the combination of mSIRPα-Fc-CD40L and anti-CD20. Supernatants from cultures were collected 24 hours after culture, incubated with QUANTI-Luc reagent (InvivoGen, catalog no. rep-qlc1; according to their recommendations), and read on a luminometer (Promega).

Tumor model systems

For CT26, A20, and WEHI3 studies, BALB/C mice were subcutaneously implanted with 5×10^5 (CT26 and A20) or 1×10^6 (WEHI3) tumor cells in 100 μL of PBS, into the rear flank, respectively, on day 0. On treatment days (treatment schematics shown in figures and described in figure legends), tumor bearing mice were randomized and either untreated or treated via intraperitoneal injection with the mSIRPα-Fc-CD40L ARC, or anti-CD40 (clone FGK4.5), anti-CD47 (clone MIAP301), anti-CD20 (clone AISB12), anti-PD-1 (clone RMP1-14), or anti-CTLA4 (clone 9D9). All test agents were diluted in PBS and injected in volumes between 100 and 200 μL. All therapeutic antibodies are from BioXcell. Tumor volume (mm^3) and overall survival was assessed throughout the time-course. Survival criteria included total tumor volume less than 1,700 mm^3 with no sign of tumor ulceration. Complete responders, in which tumors established and were subsequently rejected, are listed in the appropriate figures. Cohorts of CT26 experimental mice were euthanized between days 11 and 13 for immune profiling in splenocytes and tumor tissue using flow cytometry. Tumors were excised from these mice and dissociated using a tumor dissociation kit (Miltenyi Biotec, catalog no. 130-096-730). Tumors were excised, combined with the dissociation reagent, and then minced with a razor. The resulting slurry was transferred to a 1.5 mL Eppendorf tube and placed in a 37°C shaker for 30 minutes. During this period, the slurry was pipetted up and down every 10 minutes to break up larger pieces. Dissociated cells were homogenized through a 100-μm strainer to isolate tumor cells and infiltrating immune cells. Experimental group sizes are described in each figure legend and come from a minimum of two independent experiments.

For CD4, CD8, and IFNAR1 depletion experiments, mice were treated via intraperitoneal injection of 100 μg of anti-CD4 (clone GK1.5), 100 μg of anti-CD8 (clone 2.43), or 500 μg of anti-IFNAR1 (clone MAR1-5A3) on the schedules described in the appropriate figures (all antibodies are from BioXcell). Antibodies were diluted in

Published OnlineFirst December 18, 2019; DOI: 10.1158/2326-6066.CIR-19-0493

PBS and injected in volumes of 100 μL. CD4, CD8, and IFNAR1 populations in the peripheral blood were assessed at several time points to verify depletion and were normalized to untreated mice. Peripheral blood from WEHI3-bearing mice treated on days 7, 9, and 11 with 300 μg SIRPα-Fc-CD40L ± anti-IFNAR1 was collected, the RBCs lysed, and the resulting mononuclear cells (MNC) assessed by flow cytometry with fluorescently conjugated antibodies to CD45, CD11c, CD20, CD4, and CD8 (antibodies from BioLegend).

Safety studies

Nonhuman primate studies

Naïve cynomolgus macaques (2–4 years of age) were given SIRPα-Fc-CD40L by intravenous infusion every week, for 5 consecutive weeks, at doses of 0.1, 1, 10, and 40 mg/kg. Hematology and clinical chemistry parameters were collected by venipuncture before and after each dose. CD47 expression on circulating RBCs was assessed by flow cytometry. MNCs and serum were isolated from whole blood using Ficoll gradient separation. The resulting erythroid pellet was stained with anti-CD47 and pregated using forward/side scatter to isolate a majority RBC population. All studies were conducted at Charles River Laboratories in accordance with Institutional Animal Care and Use Committee (IACUC) guidelines.

Experimental animal guidelines

All animal studies have been conducted in accordance with, and with the approval of an IACUC and reviewed and approved by a licensed veterinarian. Experimental mice were monitored daily and euthanized by CO_2 asphyxiation and cervical dislocation prior to any signs of distress.

Statistical analysis

GraphPad Prism was used to plot and generate all graphs throughout; as well as automatically calculate error and significance. Experimental replicates (N) are shown in figures and figure legends. Unless noted otherwise, values plotted represent the mean from a minimum of three distinct experiments and error is SEM. Statistical significance (P value) was determined using unpaired t tests or one-way ANOVA with multiple comparisons. Significant P values are labeled with one or more "*", denoting *, $P < 0.05$; **, $P < 0.01$; ***, $P < 0.001$; and ****, $P < 0.0001$. Mantel–Cox statistical tests were used to determine the significance between the survival curves. P values are noted in the legends to these figures.

Results

Production and characterization of SIRPα-Fc-CD40L

The ECDs of SIRPα and CD40L were fused via an antibody Fc domain for both human and mouse to generate $SIRP\alpha_{ECD}$-Fc-$CD40L_{ECD}$; hereafter referred to as SIRPα-Fc-CD40L. *In silico* structural modeling predicted that each individual domain of the adjoined construct would fold in accordance with the native molecules, suggesting preservation of both binding functions (**Fig. 1A**). Purified SIRPα-Fc-CD40L was then analyzed for the presence of each individual domain by Western blotting using anti-SIRPα, anti-Fc, and anti-CD40L (**Fig. 1B**), revealing a glycosylated protein that formed a dimer under nonreducing conditions at the predicted monomeric molecular weight of 88.1 kDa. To further characterize the native state of SIRPα-Fc-CD40L in the absence of detergents, electron microscopy was performed, demonstrating that the major peak fraction contained a hexameric species (≥60% for both mouse and human), consistent to what had been previously described for TNF ligand fusion proteins (**Fig. 1C**; ref. 33). A minor peak fraction (~30%–35%) was also present, which comprised a tetrameric protein complex that had equivalent activity in the dual-binding ELISA (hexamer EC_{50} = 24.21 nmol/L, tetramer EC_{50} = 33.3 nmol/L, reference = 18.1 nmol/L). A dual-binding ELISA assay was developed to quantitatively demonstrate simultaneous binding of SIRPα to recombinant CD47 and CD40L to recombinant CD40 (**Fig. 1D**). Individual ELISAs also confirmed binding to recombinant human CD47, Fc, and CD40 (Supplementary Fig. S1A). Binding affinity studies using surface plasmon resonance (SPR; Supplementary Table S2) indicated that human SIRPα-Fc-CD40L bound with 0.628 nmol/L affinity to recombinant human CD47, 4.74 nmol/L affinity to recombinant human CD40, had undetectable binding to FcγR1a, -2b and -3b, while having preserved 2.33 nmol/L binding affinity to FcRn (**Fig. 1E**). To justify testing of human SIRPα-Fc-CD40L in nonhuman primates, high-affinity binding to recombinant cynomolgus macaque CD40 (3.24 nmol/L) and CD47 (1.7 nmol/L) were also confirmed. Finally, to confirm that SIRPα-Fc-CD40L interacted with native CD47 and CD40 in a similar manner to recombinant CD47 and CD40, CHOK1-hCD47, and CHOK1-hCD40 reporter cell lines were developed (Supplementary Fig. S1B and S1C). Flow cytometry studies using these reporter cell lines confirmed that SIRPα-Fc-CD40L bound to CHOK1-CD47 cells (31.85 nmol/L EC_{50}) and CHOK1-CD40 cells (22.48 nmol/L EC_{50}), but not to parental CHOK1 cells (**Fig. 1E**; Supplementary Fig. S1B and S1C). A functional ELISA demonstrated that SIRPα-Fc-CD40L outcompeted a commercially available single-sided SIRPα-Fc control for binding to recombinant CD47, generating an EC_{50} of 22 nmol/L, comparable with the 14 nmol/L EC_{50} produced by a commercial CD47-blocking antibody (**Fig. 1F**).

The mouse surrogate of SIRPα-Fc-CD40L (referred to as mSIRPα-Fc-CD40L) was generated to assess activity *in vivo*, and was first characterized similarly to the human ARC; including by Western blot analysis (Supplementary Fig. S1D) and dual-binding ELISA to both mouse CD47 and mouse CD40 simultaneously (Supplementary Fig. S1E).

SIRPα-Fc-CD40L functional activity–SIRPα domain

Because of the bifunctionality of SIRPα-Fc-CD40L, distinct functional assays were utilized to independently characterize the activity of both the SIRPα and CD40L domains. A common *in vitro* assay used to characterize the SIRPα/CD47 axis analyzes the ability of purified macrophages to phagocytose tumor cells (2, 34), particularly in the presence of ADCP-competent therapeutic antibodies (35). Accordingly, *in vitro* tumor cell phagocytosis assays were established to determine whether SIRPα-Fc-CD40L enhanced macrophage-mediated phagocytosis of various tumor cell lines both alone and in combination with targeted antibodies. Initially, several $CD20^{+}$ lymphoma (Toledo, Raji, Ramos) cell lines were cocultured with human monocyte–derived macrophages to identify a suitable platform for assessing phagocytosis; using three analogous approaches; (i) immunofluorescence (IF); to visualize the overlap in signal between labeled macrophages and labeled tumor cells, (ii) flow cytometry; to quantitate distinct populations of dually-positive tumors and macrophages, and (iii) live-cell imaging using the IncuCyte platform; to both visualize and quantitate macrophage-mediated phagocytosis of tumor cells–using tumor cells that were precoated with a pH-sensitive marker (pHrodo) that only fluoresces when a tumor cell is engulfed by a macrophage and enters a low pH (pH 4.5–5.5) phagosome (**Fig. 2A–E**; Supplementary Fig. S2A). All three approaches demonstrate that SIRPα-Fc-CD40L was capable of inducing phagocytosis as a monotherapy, and that this activity was significantly enhanced in $CD20^{+}$

Published OnlineFirst December 18, 2019; DOI: 10.1158/2326-6066.CIR-19-0493

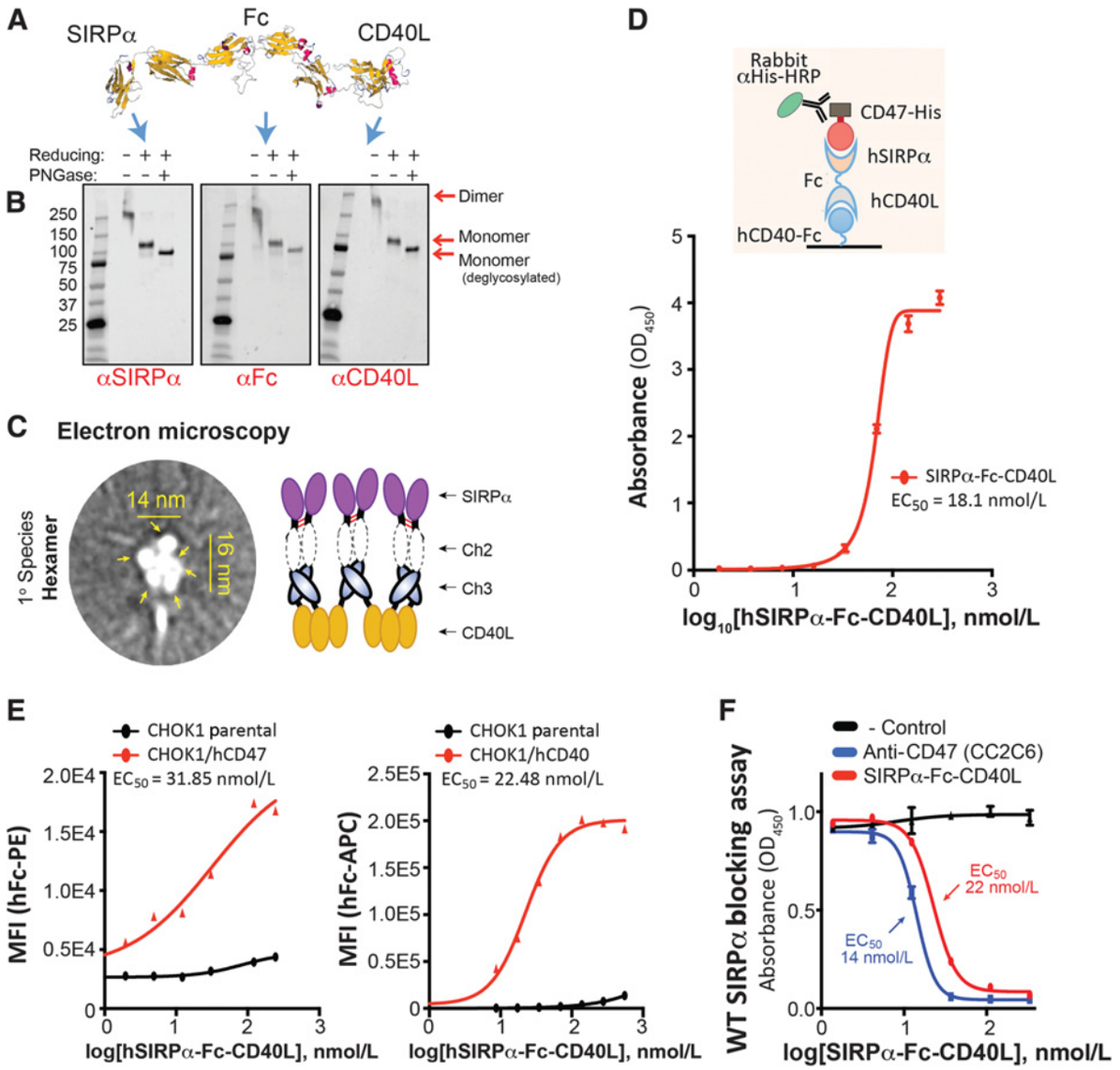

Figure 1.

SIRPα-Fc-CD40L ARC retained proper folding and binding to CD47 and CD40. **A,** Predicted tertiary structure of human SIRPα-Fc-CD40L (RaptorX; University of Chicago, Chicago, IL). **B,** Western blot analysis of SIRPα-Fc-CD40L performed by probing purified protein with human anti-SIRPα, anti-Fc, and anti-CD40L, under nonreducing and reducing conditions, and ± the deglycosylase PNGase F. **C,** Electron microscopy indicating hexameric structure of the SIRPα-Fc-CD40L drug substance. Scale is shown, and yellow arrows correspond with each identified monomer. A schematic of the hexamer species is shown to the right, depicting dimerization of the Fc domain (red lines = disulfide bonds) and trimerization of the CD40L domain. **D,** Functional dual ELISA using capture with recombinant hCD40, followed by detection with recombinant hCD47-His and then anti-His-HRP. **E,** Flow cytometry–based binding of SIRPα-Fc-CD40L to CHOK1 cells engineered to stably express human CD47 or human CD40. MFI, mean fluorescence intensity. **F,** Competition ELISA in which the disruption of binding of recombinant hSIRPα-Fc to plate-bound hCD47 was assessed in the presence or absence of hSIRPα-Fc-CD40L or a human CD47-blocking antibody (clone CC2C6).

lymphoma cells lines when combined with the ADCP-competent anti-CD20 agent, rituximab (**Fig. 2A–D**; Supplementary Fig. S2A). The phagocytosis-stimulating activity of SIRPα-Fc-CD40L/rituximab combinations was partially inhibited when Fc receptors were blocked on macrophages; however, activity was not impacted when macrophages were pretreated with a CD40-blocking antibody indicating that binding of ARC to CD40 does not contribute to phagocytosis of tumor cells.

Calreticulin on tumor cells serves as a prophagocytic signal, facilitating tumor cell phagocytosis following blockade of the CD47/SIRPα pathway (36). We demonstrated that both calreticulin and Fc receptor engagement was required for efficient phagocytosis of $CD20^+$ B-cell lymphoma cells by the combination of SIRPα-Fc-CD40L and rituximab using a calreticulin-blocking peptide, confirming the importance of Fc interactions for Fc-competent targeting antibodies and providing evidence that the initiation of phagocytosis by SIRPα-Fc-

Published OnlineFirst December 18, 2019; DOI: 10.1158/2326-6066.CIR-19-0493

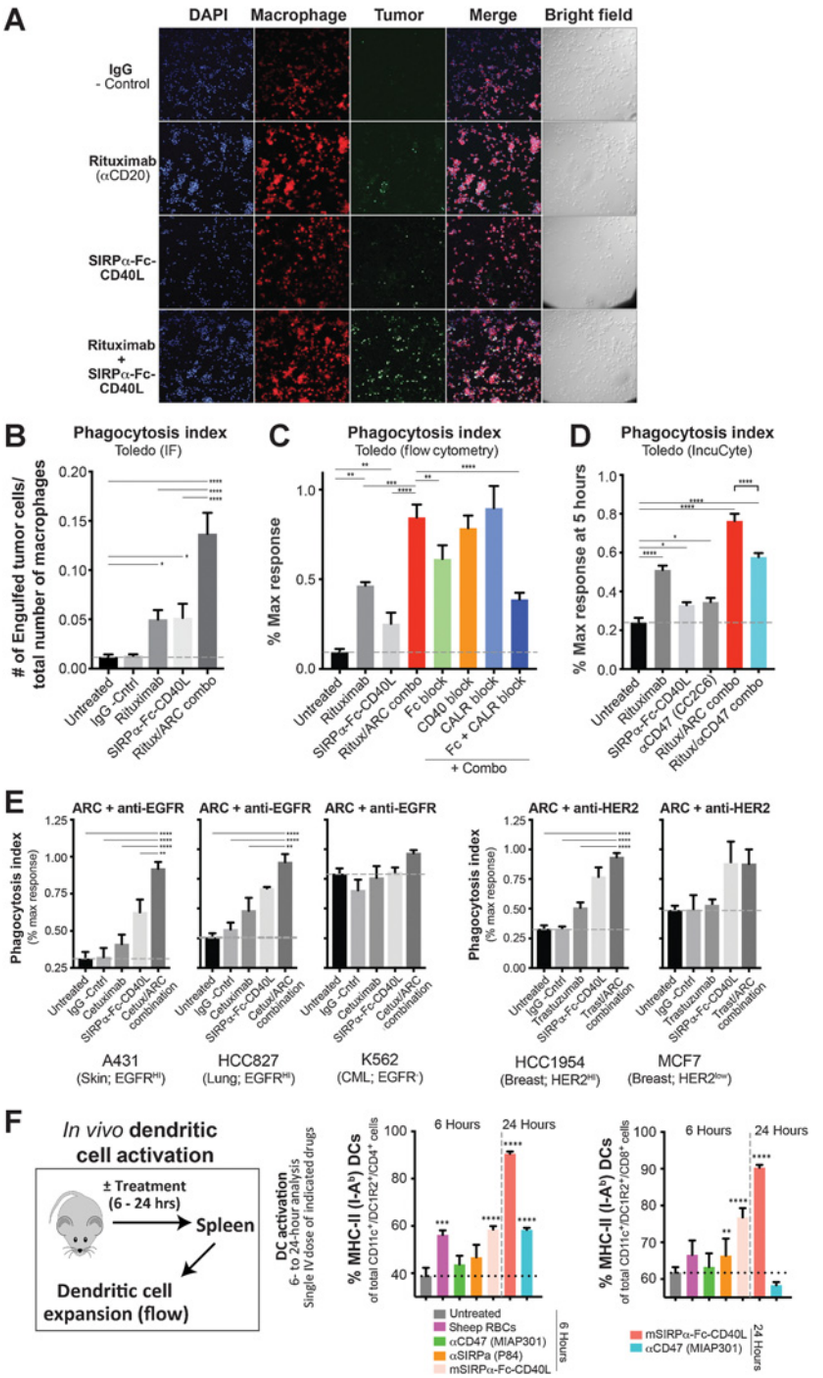

Figure 2.

SIRPα domain of SIRPα-Fc-CD40L stimulated phagocytosis *in vitro* and activation of DCs *in vivo*. **A,** Human macrophage (red)/lymphoma (Toledo; green) coculture analysis of phagocytosis using IF. DAPI was used to label nuclei (blue), and merged channels and phase images are shown to the right. The human IgG negative control was used at 0.06 μmol/L, rituximab at 0.06 μmol/L, and hSIRPα-Fc-CD40L at 1 μmol/L. **B,** The number of tumor cells engulfed per total number of macrophages was quantitated using 7 to 13 distinct IF images obtained for each of the treatment conditions. ImageJ software was used for the analysis. **C,** Human macrophages and Toledo lymphoma cell coculture phagocytosis assessed by flow cytometry; with an IgG negative control, monotherapy hSIRPα-Fc-CD40L and rituximab, or the combination of these agents; analyzed after 2 hours. Identical assays were set up where macrophages were preincubated for 1 hour with 20 μg/mL of a commercially available Fc block cocktail, with 20 μg/mL of a CD40 blocking antibody or with 5 μg/mL of a calreticulin blocking peptide. **D,** IncuCyte phRodo Red prelabeled Toledo cells were cocultured with human macrophages, and phagocytosis was assessed using time-lapse fluorescent microscopy over a course of 5 hours. Cocultures were treated with hSIRPα-Fc-CD40L (1 μmol/L), rituximab (1 μg/mL), anti-CD47 (clone CC2C6; 33 μg/mL), or with combinations of either SIRPα-Fc-CD40L and rituximab or anti-CD47 and rituximab. **E,** Flow cytometry was used to assess phagocytosis of other human tumor cell lines in response to monotherapy SIRPα-Fc-CD40L at 1 μmol/L, cetuximab/trastuzumab monotherapy at 0.06 μmol/L, or the combination of the agents in human tumor cell lines verified to express the given targets. K562 cells were used as a negative control for phagocytosis. **F,** Mice were treated with a single intravenous dose of sheep RBCs (1×10^7 cells; as a positive control), blocking antibodies to CD47 and SIRPα (100 μg each), or mSIRPα-Fc-CD40L (at 100 or 300 μg). After 6 or 24 hours, mice were euthanized and spleens excised, dissociated, and assessed by flow cytometry for populations of activated $CD4^+$ (left) or $CD8^+$ DCs (right); also positive for MHC-II ($I\text{-}A^b$), CD11c, and DC1R2. See corresponding data in Supplementary Fig. S2D–S2F.

CD40L was driven by the SIRPα domain (**Fig. 2C**). We observed similar monotherapy phagocytosis activity of SIRPα-Fc-CD40L to the CC2C6 clone of anti-CD47 (**Fig. 2D**). When both agents were combined with rituximab, the SIRPα-Fc-CD40L/rituximab combination stimulated significantly greater phagocytosis activity than the anti-CD47/rituximab combination suggesting competition by two separate therapeutics that require Fc receptor engagement. We examined the phagocytic activity in a range of human tumor cell lines using several ADCP-targeted antibodies; $EGFR^+$ melanoma (A431 cells) and lung (HCC827 cells), $EGFR^-$ chronic myelogenous leukemia (CML; K562 cells), and $HER2^+$ breast ($HCC1954^{HER2\ HI}$ and $MCF7^{HER2\ LOW}$ cells) were used to facilitate combinations with EGFR- (cetuximab) and HER2- (trastuzumab) targeted antibodies. Consistent with the lymphoma cell lines, monotherapy SIRPα-Fc-CD40L–stimulated macrophage phagocytosis, which was enhanced in combination with targeted antibodies (**Fig. 2E**; Supplementary Fig. S2B). Trastuzumab did not induce phagocytosis in the $HER2^{LOW}$ cell line MCF7; however, SIRPα-Fc-CD40L demonstrated modest monotherapy activity. We did not observe phagocytic activity of EGFR-negative K562 cells with monotherapy or combinations of SIRPα-Fc-CD40L

Published OnlineFirst December 18, 2019; DOI: 10.1158/2326-6066.CIR-19-0493

with cetuximab (**Fig. 2E**). Similar phagocytic activity was observed using the mouse surrogate mSIRPα-Fc-CD40L to treat cocultures of BMDMs and either A20 or WEHI3 cells (Supplementary Fig. S1F). Interestingly, a higher phagocytosis index was generated using mSIRPα-Fc-CD40L, as compared with a mouse CD47-blocking antibody.

Finally, using an *in* vivo mouse assay that examines the activation status of splenic DCs in response to SIRPα/CD47 inhibitors or sheep RBCs (5), we observed that intravenous administration of sheep RBCs, CD47 blocking antibodies, or SIRPα blocking antibodies all stimulated upregulation of both activated $CD4^+$ and $CD8\alpha^+$ DCs that were positive for MHC-II within 6 hours (**Fig. 2F**; Supplementary Fig. S2D–S2F). Similarly, administration of mouse SIRPα-Fc-CD40L also upregulated surface expression of MHC-II, CD80, and CD86 on splenic $CD4^+$ and $CD8\alpha^+$ in a higher proportion of overall splenic DCs than was observed in the antibody-treated groups.

SIRPα-Fc-CD40L functional activity–CD40L domain

On the basis of the reported role of NIK signaling for CD40-dependent cross-priming, functionality of the CD40L domain of SIRPα-Fc-CD40L was evaluated using two different CD40-dependent NFκB/NIK reporter systems (**Fig. 3A** and **B**; refs. 37, 38). These data indicated that SIRPα-Fc-CD40L had similar activity to a single-sided CD40L fusion protein in both reporter systems. SIRPα-Fc-CD40L was present in a soluble form in both assays, and no Fc receptor or other cross-linking agents were present. Along these lines, a CD40 agonist antibody was unable to stimulate NIK/NFκB activity in the same system in the absence of an accessory cell that can provide Fc receptor engagement (**Fig. 3B**). These data indicated that SIRPα-Fc-CD40L can stimulate CD40 signaling in the absence of cross-linking, likely due to its inherent hexameric configuration. Similar observations were made using mSIRPα-Fc-CD40L in comparison with a mouse CD40 agonist antibody (Supplementary Fig. S1G).

The observation that SIRPα-Fc-CD40L stimulated CD40 signaling prompted investigation of other cellular functions that depend on CD40 signaling. CD40 stimulates proliferation of B cells and $CD4^+$ T cells from human PBMCs in the presence of cross-linked anti-CD40 antibodies or CD40L (39, 40). To investigate this readout, $CD8^+$ T-cell–depleted PBMCs were isolated from a total of 33–50 different human donors and cultured in the presence of a dose titration of SIRPα-Fc-CD40L (**Fig. 3C** and **D**; Supplementary Fig. S3A). As compared with a media-only negative control and a KLH-positive control, soluble SIRPα-Fc-CD40L stimulated dose-dependent proliferation of human PBMCs over a 7-day culture (**Fig. 3C**), and a dose-dependent increase in the number of IL2-secreting PBMC on day 8 of the culture (**Fig. 3D**), previously reported as a downstream event of CD40 activation (41).

The activation status of macrophages from SIRPα-Fc-CD40L–treated macrophage:Toledo lymphoma cell cocultures was assessed by qRT-PCR for expression of the type I IFN-regulatory genes IFNα1 and IFNβ1, and the macrophage activation markers CD80 and CD86 (**Fig. 3E**). Monotherapy SIRPα-Fc-CD40L and rituximab (anti-CD20) induced macrophage activation and the expression of type I IFN genes in the isolated macrophages, which was enhanced when the two agents were combined. Similar results were observed in macrophages isolated after coculture with Raji cells in the presence of SIRPα-Fc-CD40L, rituximab, or the combination (Supplementary Fig. S3B).

A macrophage reporter system (RAW264.7 ISG) was utilized to determine activation of a type I IFN response by mSIRPα-Fc-CD40L. When RAW264.7 ISG cells were cocultured with A20 lymphoma cells, mSIRPα-Fc-CD40L stimulated an increase in IFN gene-driven luciferase activity (**Fig. 3F**). Commercially available recombinant murine Fc-CD40L was also able to stimulate IFN production; however, no significant signal was observed using a recombinant single-sided SIRPα-Fc protein indicating that type I IFN-activation acted downstream and independently from tumor cell phagocytosis, through CD40 engagement (**Fig. 3F**). A murine rituximab surrogate (anti-CD20) induced some monotherapy IFN response and significantly amplified the monotherapy signal seen with mSIRPα-Fc-CD40L (**Fig. 3F**) providing additional rationale for the combination of SIRPα-Fc-CD40L with targeted ADCP-competent antibodies. Such combinations may have had the ability to increase tumor cell phagocytosis and initiate pathways capable of activating APC and enhancing antigen processing/presentation. These data indicated that the magnitude of the type I IFN response could be enhanced when SIRPα and CD40L were physically linked to one another.

Antitumor activity of murine SIRPα-Fc-CD40L

The syngeneic CT26 colon tumor model was used to provide an initial assessment of the antitumor activity of murine SIRPα-Fc-CD40L in comparison with CD40 agonist and CD47-blocking antibodies. Implanted CT26 tumors were grown to approximately 30 mm^3 before treatment was initiated with a fixed regimen of two doses of either CD40 agonist antibody (clone FGK4.5), CD47-blocking antibody (clone MIAP301), a combination of both antibodies or murine SIRPα-Fc-CD40L. As compared with vehicle controls, both CD40 agonist and CD47-blocking antibodies provided moderate extensions in tumor growth, with 25% of mice completely rejecting primary tumors in the CD40 agonist monotherapy group (**Fig. 4A**). Mice treated with a combination of CD40 and CD47 antibodies were observed to have a longer delay in tumor outgrowth and 33% of mice rejected tumors. In comparison with the antibody groups, complete tumor rejection was observed in 50% of the mice treated with mSIRPα-Fc-CD40L, along with significant tumor growth delay and prolonged survival (Mantel–Cox test, $P = 0.0364$ vs. anti-CD40/anti-CD47 combination group) in the remaining mice. A majority of the mice that rejected the primary tumor rejected a secondary tumor challenge in the absence of additional treatment (60%; **Fig. 4A**). In both the antibody combination and mSIRPα-Fc-CD40L–treated groups, there was an increase in the proportion of AH1-tetramer (specific for the MHC $H\text{-}2L^d$–restricted immunodominant epitope of gp70 expressed by the CT26 tumor cell line) $CD8^+$ T cells in both the tumor and spleen (**Fig. 4B**; Supplementary Fig. S4A). To determine whether these T-cell responses contributed to therapeutic efficacy, we repeated these studies in $CD4^+$ and $CD8^+$ T-cell antibody–depleted mice (**Fig. 4C**; Supplementary Figs. S3A and S4B–S4D). $CD4^+$ T cells were partially required for therapeutic efficacy, whereas the loss of $CD8^+$ cells completely eliminated the therapeutic benefit of mSIRPα-Fc-CD40L, similar to CD47-blocking antibodies (11, 12). CD8 depletion following the initiation of mSIRPα-Fc-CD40L therapy partially abrogated the observed antitumor efficacy (Supplementary Fig. S4D).

CD47-blocking antibodies plus rituximab potentiate macrophage-mediated phagocytosis, correlating to the combination's promising clinical efficacy in patients with late-stage diffuse large B-cell lymphoma (42, 43). Because SIRPα-Fc-CD40L potentiated the activity of rituximab, we investigated the combination of SIRPα-Fc-CD40L with a murine surrogate for rituximab (anti-mouse CD20; clone AISB12) in two $CD20^+$ mouse tumor models, WEHI3 and A20. In both tumor models, we observed similar control of established tumor growth when anti-CD20 antibodies or mSIRPα-Fc-CD40L were tested as

Published OnlineFirst December 18, 2019; DOI: 10.1158/2326-6066.CIR-19-0493

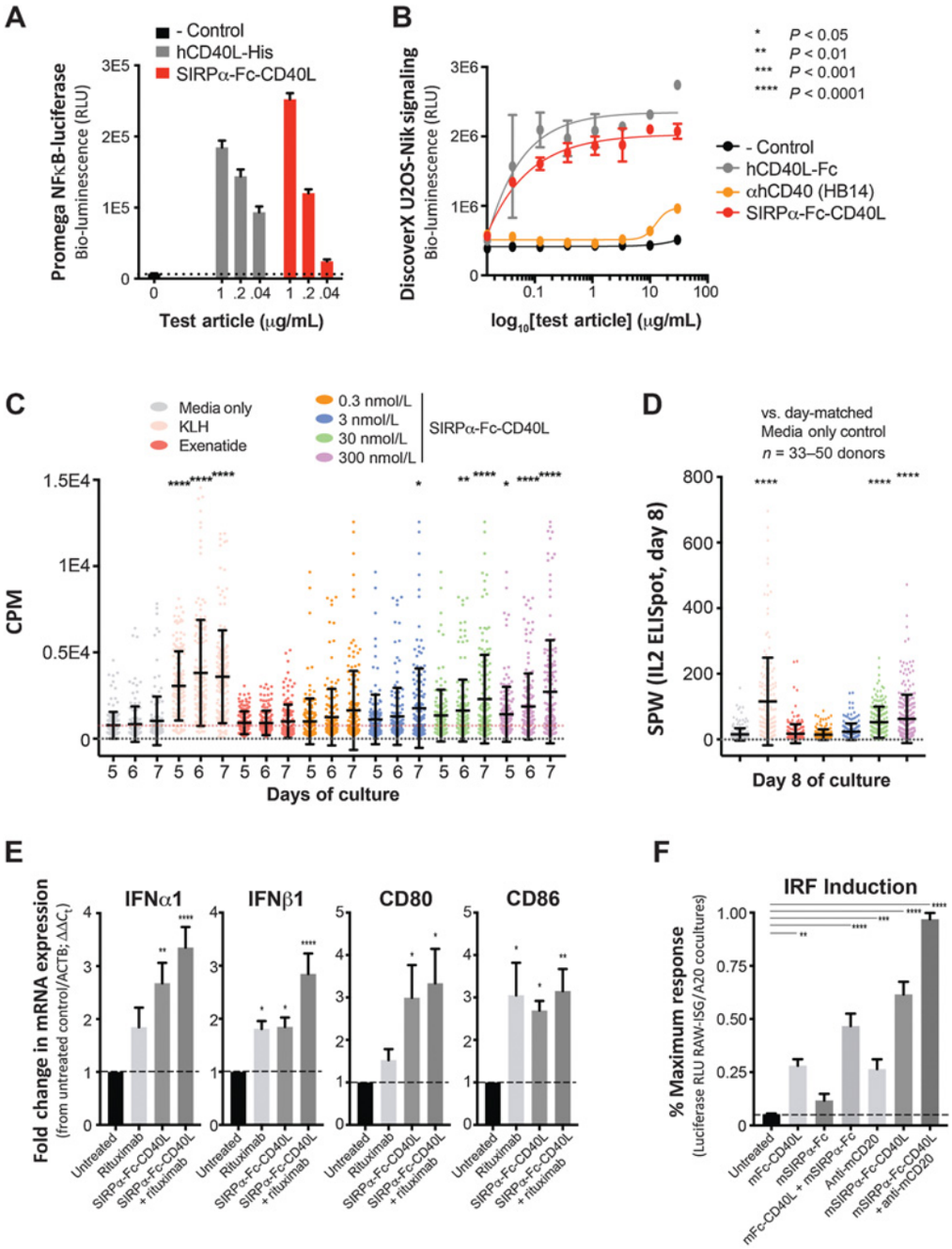

Figure 3.

CD40L domain of SIRPα-Fc-CD40L induced NFκB signaling, antigen-independent PBMC activation, and a type I IFN response. **A,** Human SIRPα-Fc-CD40L stimulated canonical NFκB signaling in CHO-K1/hCD40/NFκB reporter cells. Shown is luminescence after 6 hours. Recombinant human CD40L-His serves as a positive control. **B,** Noncanonical NIK/NFκB reporter U2OS cells (expressing human CD40) were cultured with a titration of recombinant hCD40L-Fc, an agonist hCD40 antibody, or SIRPα-Fc-CD40L. Shown is luminescence after 6 hours. CD8-depleted PBMCs from 33 to 50 distinct human donors were cultured with media only, the neoantigen positive control KLH, the clinical stage nonactivating control exenatide, or 0.3, 3, 30, or 300 nmol/L of hSIRPα-Fc-CD40L. **C,** On days 5, 6, and 7, proliferation was assessed via [^{3}H]-Thymidine incorporation. **D,** On day 8, IL2-positive cells were assessed by ELISpot. **E,** *IFNα1, IFNβ1, CD80*, and *CD86* gene expression from macrophages harvested from macrophage:Toledo lymphoma cell cocultures in phagocytosis assays in the presence of rituximab (0.06 μmol/L), hSIRPα-Fc-CD40L (1 μmol/L), or the combination of both agents. **F,** RAW 264.7-Lucia ISG cells were cocultured with A20 lymphoma cells in the presence of 50 μg/mL of mSIRPα-Fc-CD40L, recombinant Fc-mCD40L, mSIRPα-Fc, or their combination or 1 μg/mL anti-mCD20, or the combination of mSIRPα-Fc-CD40L and anti-mCD20. After 24 hours, type I IFN–induced luminescence was assessed using a luminometer. The maximum signal of luminescence across all experiments was set to 1, and all other values were normalized accordingly.

Published OnlineFirst December 18, 2019; DOI: 10.1158/2326-6066.CIR-19-0493

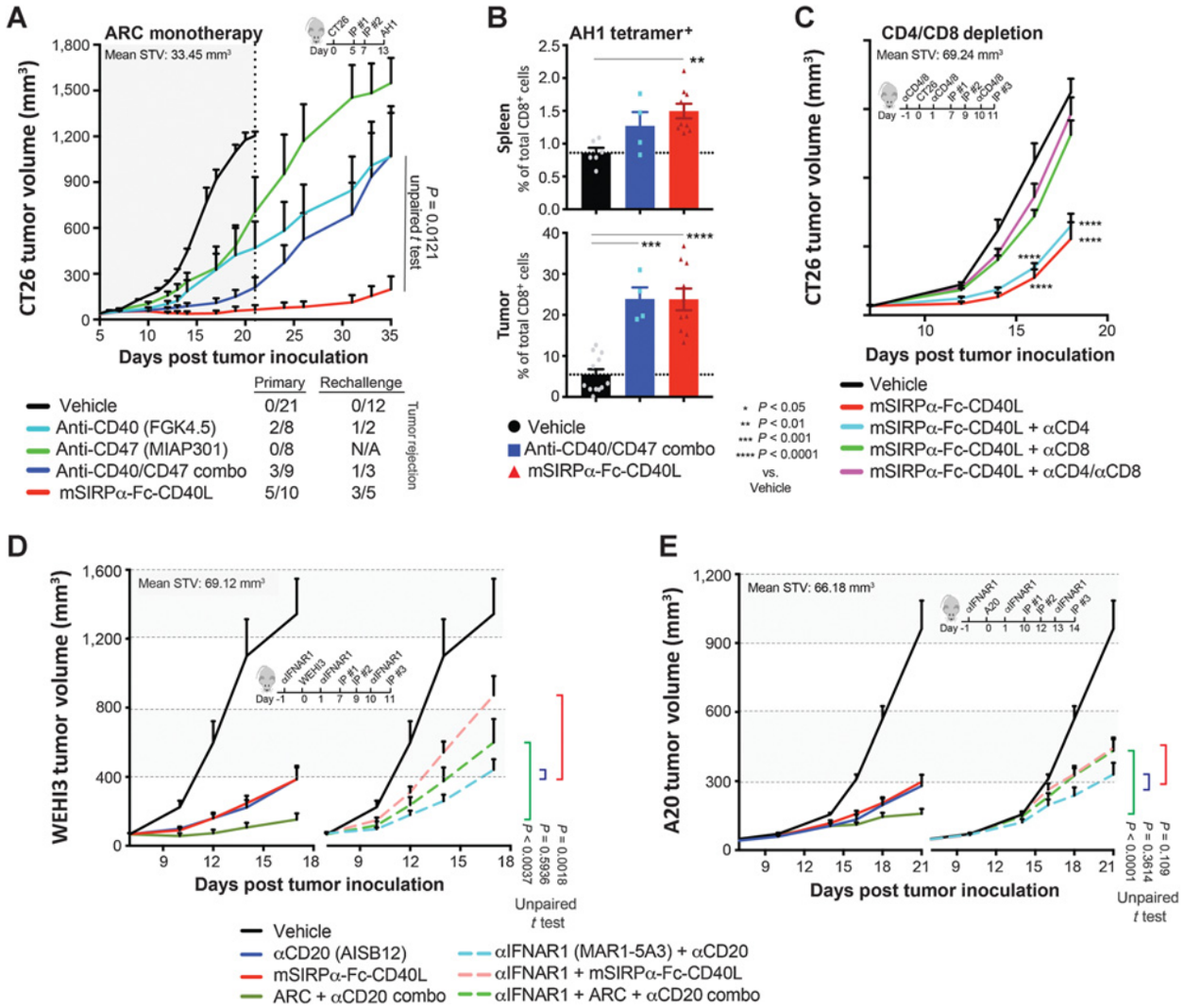

Figure 4.

Antitumor efficacy of the murine SIRPα-Fc-CD40L surrogate. **A,** CT26 tumor growth curves of mice treated with two doses of vehicle (PBS; $n = 21$), anti-CD40 (clone FGK4.5; $n = 8$), anti-CD47 (clone MIAP301; $n = 8$), the combination of both antibodies ($n = 9$; 100 μg per antibody, per dose), or mSIRPα-Fc-CD40L (150–300 μg per dose; $n = 10$). STV stands for "starting tumor volume" on the day that treatment began. **B,** The percentage of AH1 antigen-specific $CD8^+$ T cells in the spleens and tumors using tetramer reagents. **C,** CT26 tumor growth curves in mice predepleted of CD4, CD8, or both CD4 and CD8 cells prior to the initiation of treatment with vehicle (PBS; $n = 10$) or mSIRPα-Fc-CD40L ARC ($n = 10$; 300 μg per dose) on days 7, 9, and 11. Tumor growth curves of WEHI3 (**D**) or A20 tumors (**E**) in mice treated with vehicle (PBS; $n = 11$ mice in each tumor model), anti-CD20 (100 μg per dose; $n = 9$ in A20 and $n = 10$ in WEHI3), mSIRPα-Fc-CD40L (300 μg per dose; $n = 11$ in A20 and $n = 10$ in WEHI3), or the combination of mSIRPα-Fc-CD40L and anti-CD20 ($n = 10$ in A20 and $n = 9$ in WEHI3) on days 7, 9, and 11 (WEHI3) or days 10, 12, and 14 (A20); when tumors were established and reached approximately 65 to 70 mm^3. Also shown are tumor growth curves in mice predepleted of IFNAR1 cells prior to the initiation of treatment. Groups included anti-CD20 ($n = 10$ in both tumor models), mSIRPα-Fc-CD40L ($n = 12$ in A20 and $n = 11$ in WEHI3), or the combination of the two agents ($n = 10$ in A20 and $n = 8$ in WEHI3).

monotherapies (**Fig. 4D** and **E**). We observed additive control of tumor growth when anti-CD20 antibodies and mSIRPα-Fc-CD40L were combined as compared with anti-CD20 monotherapy in A20 ($P = 0.0302$) and WEHI ($P = 0.0166$) or mSIRPα-Fc-CD40L monotherapy in A20 ($P = 0.0017$) and WEHI (0.0095). Next, we sought to explore our previous *in vitro* findings implicating SIRPα-Fc-CD40L in type I IFN activation in an *in vivo* setting and assessed the impact of an IFNα receptor 1 (IFNAR1) blocking antibody on antitumor efficacy. Antibody-mediated blockade of IFNAR1 significantly reduced the efficacy of mSIRPα-Fc-CD40L both alone and in combination with anti-CD20 in mice bearing established WEHI3 tumors (**Fig. 4D** and **E**; Supplementary Fig. S4C and S4E). IFNAR1 blockade most significantly impacted mSIRPα-Fc-CD40L–treated groups, with less effect on anti-CD20 monotherapy–treated mice. Consistent with this observation, tumor control was similar between anti-CD20 monotherapy and in combination with mSIRPα-Fc-CD40L; indicating that a majority of the combinatorial benefit required a functional type I IFN response. When depletion of IFNAR1 was initiated following initial treatment with mSIRPα-Fc-CD40L, there was only marginal (WEHI3) or no (A20) acceleration in tumor growth, indicating that

Published OnlineFirst December 18, 2019; DOI: 10.1158/2326-6066.CIR-19-0493

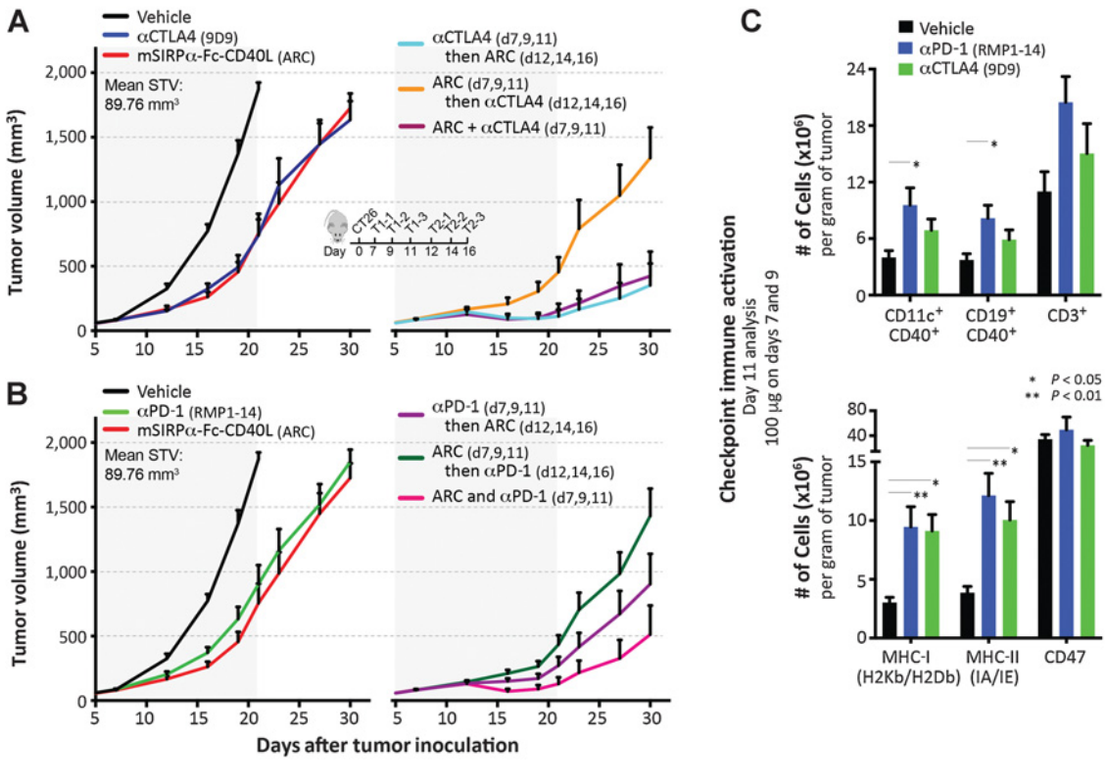

Figure 5.

mSIRPα-Fc-CD40L exhibited improved antitumor efficacy when combined with anti-CTLA4 or anti-PD-1. **A** and **B,** Tumor growth curves of mice bearing larger CT26 tumors [mean starting tumor volume (STV) 89.76 mm^3] after treatment with anti-CTLA4 (clone 9D9; **A**) and anti-PD-1 (clone RMP1–14; **B**) either dosed before mSIRPα-Fc-CD40L (on days 7, 9, and 11 with ARC on days 12, 14, and 16), after mSIRPα-Fc-CD40L (on days 12, 14, and 16 with ARC on days 7, 9, and 11), or simultaneously with mSIRPα-Fc-CD40L (on days 7, 9, and 11). Experimental replicates are shown in Supplementary Fig. S5A and S5C. **C,** Day 11 CT26 tumor and infiltrating leukocyte phenotyping by flow cytometry in mice treated with two intraperitoneal doses of 100 μg of either anti-CTLA4 or anti-PD-1 given on days 7 and 9. Cell populations were assessed for $CD40^+$ DCs ($CD11c^+$), B cells ($CD19^+$), and T cells ($CD3^+$; top) and MHC-I, MHC-II, and $CD47^+$ cells (bottom) based on cell counts and tumor weights taken at harvest.

IFNAR1 signaling functions very early following treatment with mSIRPα-Fc-CD40L (Supplementary Fig. S4E).

As the efficacy of SIRPα-Fc-CD40L was immune-mediated, we hypothesized that CTLA4- and PD-1–blocking antibodies may improve the antitumor effects of SIRPα-Fc-CD40L. To study these combinations, CT26 tumors grown to approximately 89 mm^3 were treated with a fixed regimen of three doses of mSIRPα-Fc-CD40L combined with three doses of CTLA4- or PD-1–blocking antibodies in different sequences (**Fig. 5A** and **B**). The larger starting tumor volumes were selected so that the monotherapy activity of both treatments would be reduced to observe additive or synergistic effects of the combination. mSIRPα-Fc-CD40L had similar antitumor efficacy to anti-CTLA4 or anti-PD-1 antibodies (**Fig. 5A** and **B**); however SIRPα-Fc-CD40L antitumor efficacy was significantly improved when given together with anti-CTLA4 (57% rejection), together with anti-PD-1 (50% rejection), following anti-CTLA4 (58.8% rejection), or following anti-PD-1 (25% rejection; **Fig. 5A** and **B**; Supplementary Fig. S5A–S5D). Nearly all of the mice that rejected the primary CT26 tumor, rejected a secondary tumor challenge compared with naïve mice (Supplementary Fig. S5A–S5D).

Checkpoint blockade of PD-1 and CTLA4 can enhance the antitumor activity of immunotherapeutics with immune-priming activity, including CD40 agonists (44). To understand the mechanistic basis for synergy between PD-1/CTLA4 blockade and mSIRPα-Fc-CD40L, we excised CT26 tumors from anti-PD-1– or anti-CTLA4–treated mice 11 days after inoculation and performed phenotypic analysis of the tumor-infiltrating lymphocytes. Both agents expanded $CD40^+$ dendritic cells/B cells and $CD3^+$ T cells, and induced the upregulation of MHC-I and MHC-II (**Fig. 5C**). Thus, initial treatment with anti-PD-1 or anti-CTLA4 stimulated expansion of CD40-expressing immune cells potentially explaining the improved responsiveness with mSIRPα-Fc-CD40L. Checkpoint inhibitor blockade did not affect the tumor surface expression of CD47 (**Fig. 5C**; Supplementary Fig. S5E), suggesting that checkpoint combination synergy functions independently of phagocytosis activity.

Safety and activity of SIRPα-Fc-CD40L in nonhuman primates

Enthusiasm surrounding the clinical utility of SIRPα/CD47 inhibition is somewhat tempered by expression of CD47 on erythrocytes and platelets, and the associated risk of hemolysis and thrombocytopenia (21, 42, 45). The Fc domain of hSIRPα-Fc-CD40L does not bind effector Fc receptors (Supplementary Table S2), and *in vitro* studies did not reveal evidence of hemolysis in human or cynomolgus macaque erythrocytes (Supplementary Fig. S6B); however, the *in vitro* systems used to test this question had significant limitations, including a complete lack of macrophages. Thus, a more accurate measure of

Published OnlineFirst December 18, 2019; DOI: 10.1158/2326-6066.CIR-19-0493

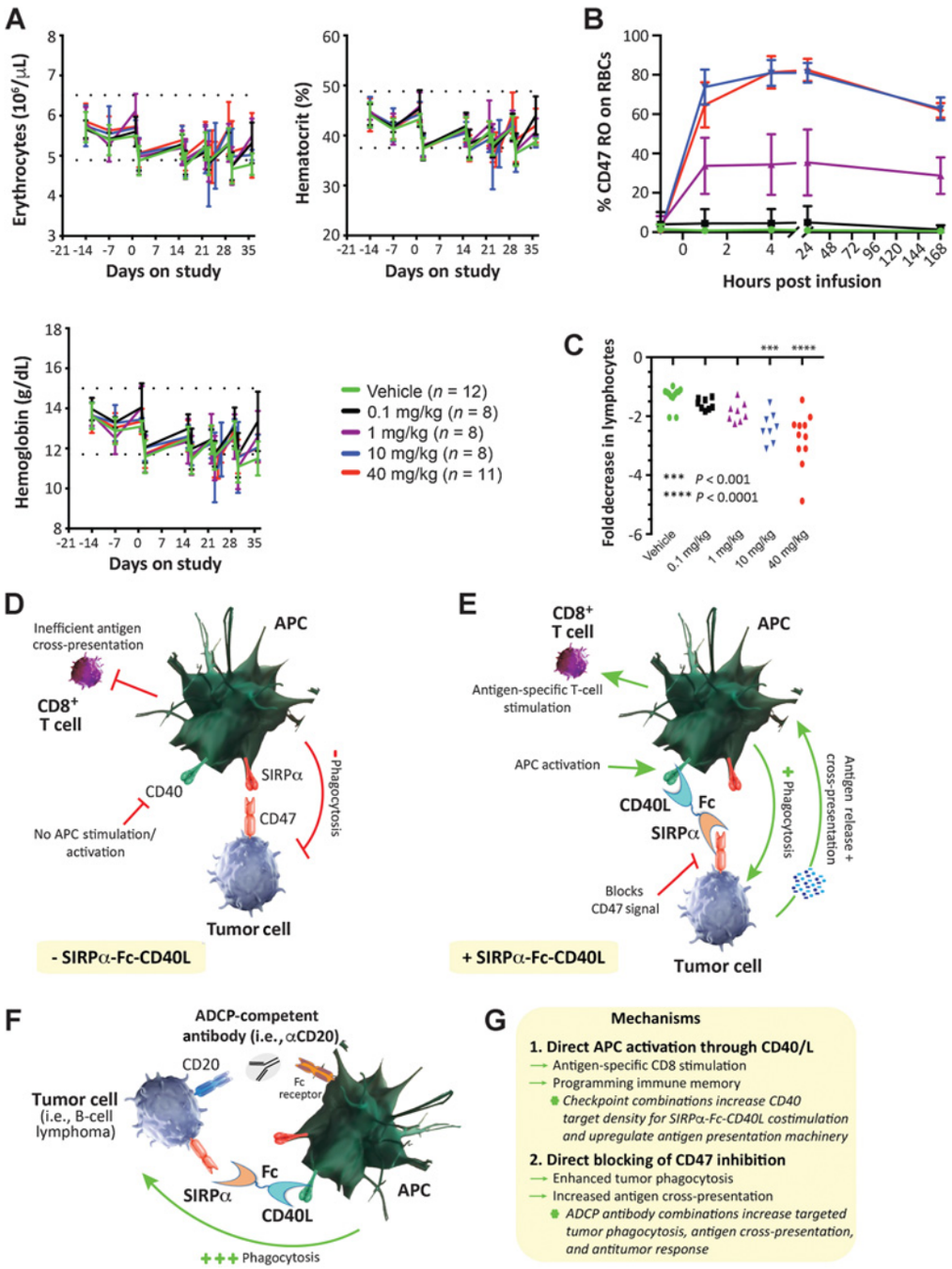

Figure 6.

hSIRPα-Fc-CD40L safety in cynomolgus macaques and overall mechanism of action. **A,** Cynomolgus macaques were treated with vehicle or 0.1, 1, 10, and 40 mg/kg of SIRPα-Fc-CD40L. Blood chemistry analysis assessed peripheral erythrocyte counts, hemoglobin levels, and hematocrit. **B,** CD47 receptor occupancy was assessed following the first dose by flow cytometry. Plotted is the inverse of the Free-CD47 flow cytometry signal, since the loss in detectable CD47 signal with increasing dose is directly proportional to the percentage of cells whose CD47 receptor is already bound by hSIRPα-Fc-CD40L. **C,** The fold change in peripheral lymphocyte count from predose to 24 hours postdose is shown. **D–G,** The proposed mechanism of action of SIRPα-Fc-CD40L. **D,** Tumor-expressed CD47 can provide a "do not eat me" signal to APCs through the binding of SIRPα. **E,** SIRPα-Fc-CD40L can relieve this inhibitory signal while simultaneously providing an "eat me" signal via costimulation of CD40 by CD40L. This enhances tumor phagocytosis, APC activation, increased antigen processing/presentation, and induction of an antitumor antigen-specific $CD8^+$ T-cell response. **F** and **G,** Combining SIRPα-Fc-CD40L with targeted ADCP-competent antibodies potentiates their phagocytosis activity.

Published OnlineFirst December 18, 2019; DOI: 10.1158/2326-6066.CIR-19-0493

hematologic toxicities required *in vivo* dosing in a relevant animal model.

Cynomolgus macaques are a relevant species for evaluating SIRPα/CD47-related toxicity due to high homology of CD47 between human and cynomolgus macaque (98.69% identity) and the development of the priming dose strategy for the CD47-specific Hu5F9-G4 antibody (46). We confirmed species cross-reactivity of hSIRPα-Fc-CD40L with recombinant cynomolgus CD47 (1.7 nmol/L binding affinity) and CD40 (3.24 nmol/L binding affinity). We sought to test the safety and activity of hSIRPα-Fc-CD40L following repeat doses in cynomolgus macaques. There was no evidence of hemolysis or thrombocytopenia following repeated infusion with hSIRPα-Fc-CD40L at doses up to 40 mg/kg over the course of the study (**Fig. 6A**). Mild declines in hematology parameters were noted; however, these declines were also noted in the vehicle control group and were most likely related to procedural effects and repeated blood collections. Dose-dependent receptor occupancy was observed across the dosing groups which peaked 4 hours postinfusion at 80.96% ± 2.6%, and was roughly equivalent between the 10 and 40 mg/kg dose groups (**Fig. 6B**; Supplementary Fig. S6A). CD47 occupancy was stable and remained at 62.78% ± 2.3% occupancy on RBC CD47 when evaluated 168 hours postinfusion (**Fig. 6B**). We also observed dose-dependent episodic fluctuation in the total number of lymphocytes before and after each dose, which were of lower magnitude than the postdose reductions observed for circulating $CD40^+$ lymphocytes (**Fig. 6C**). This peripheral decrease in $CD40^+$ B cells was consistent with similar observations seen in the blood of mice treated with mSIRPα-Fc-CD40L (Supplementary Fig. S6C–S6F). In mice, the decrease in B cells was dose dependent, plateaued at a single intraperitoneal dose of 150 μg, and was accompanied by a significant increase in $CD8^+$ DCs (Supplementary Fig. S6C–S6F). Finally, we observed dose-dependent increases in multiple serum cytokines/chemokines in cynomolgus macaques following each infusion of hSIRPα-Fc-CD40L, including CCL2, CXCL9, CXCL10, IFNα, IL6, IL15, and IL23 (Supplementary Table S3), suggestive of an on-target pharmacodynamic biology. The overall mechanism through which SIRPα-Fc-CD40L is proposed to bridge macrophage-mediated tumor cell phagocytosis to APC activation and antigen presentation is outlined in **Fig. 6D–G**.

Discussion

The description of CD47 as a "do not eat me" signal in a broad range of cancers stimulated exploration of what combinations of "eat me" signals may enhance antitumor immunity in the setting of CD47 blockade (10, 47, 48). Preclinical combinations of CD47 blockade and ADCP-competent antibodies, including rituximab and trastuzumab, enhance tumor phagocytosis (25, 35, 36, 42, 49). At least 50% of patients with relapsed or refractory diffuse large B-cell lymphoma or follicular lymphoma treated with Hu5F9-G4, a humanized, IgG4 isotype, CD47-blocking mAb, in combination with rituximab demonstrate objective responses (42). CD47 blockade enhances antigen presentation in immune-neglected tumors (50), yet only sporadic clinical responses have been observed using CD47/SIRPα blocking therapeutics as monotherapy or in combination with PD-1/L1–blocking antibodies. Thus, we sought to determine whether the addition of CD40L could enhance APC activation, antigen presentation, and antitumor immunity downstream of CD47/SIRPα blockade using a single fusion protein containing both SIRPα and CD40L.

Given the oligomeric nature of SIRPα-Fc-CD40L, it was important to independently characterize the functionality of both the SIRPα and CD40L domains. Our data demonstrated that the SIRPα domain functioned as expected by binding to CD47 with high affinity and potentiating macrophage-mediated phagocytosis alone and in the presence of multiple ADCP-competent antibodies. Similarly, the CD40L domain activated both canonical and noncanonical NFκB signaling, and stimulated human PBMC proliferation and IL2 secretion *in vitro*. CD47 blockade induces a type I IFN response following uptake of tumor mitochondrial DNA, leading to effective antitumor immunity (12). Similarly, SIRPα-Fc-CD40L directly stimulated a type I IFN response, effects not observed with SIRPα-Fc fusion proteins or CD47-blocking antibodies. Such findings could obviate the need for additional type I IFN or STING agonists to enhance antitumor immunity.

While *in vitro* assays tend to favor the biology of either the SIRPα or CD40L domains (i.e., NFκB reporter assays primarily inform on CD40 activation, whereas macrophage phagocytosis assays primarily inform on SIRPα/CD47 blockade), *in vivo* studies provided a more complete view of the overall functionality of the construct. SIRPα-Fc-CD40L significantly improved rejection of both primary and secondary tumors as compared with individual antibodies targeting CD40 and CD47 used alone or in combination, similar to PD-1-Fc-OX40L (29). The observation of enhanced antitumor immunity cannot be fully explained by the AH1-tetramer–positive CD8 T-cell population; however, it is possible that other clonotypes were activated that were not detected by the AH1 tetramer, which is consistent with the observation that $CD8^-$ depletion eliminated antitumor immunity. It is also possible that the cytolytic activity of individual tumor specific $CD8^+$ T-cell clones was enhanced, which is under continued investigation.

Additional evidence for SIRPα-Fc-CD40L bridging an innate and adaptive immune response was provided by the observation that antitumor immunity was dependent both on type I IFNs and T cells *in vivo*. The T-cell–mediated immune responses downstream of CD47/SIRPα blockade may have been restrained by immune checkpoints. Accordingly, the sequencing of these antibodies with SIRPα-Fc-CD40L had a dramatic influence on the control and rejection of established tumors. Pretreatment with anti-CTLA4 or anti-PD-1 increased the proportion of $CD40^+$ DCs and B cells within tumor-infiltrating leukocytes, providing possible mechanistic insight that could explain the antitumor benefit when CD40L was also present. Further exploration of SIRPα-Fc-CD40L in combination with checkpoint inhibitors is thus warranted.

These data suggest that while CD47 blockade is an effective strategy to enhance macrophage mediated tumor cell phagocytosis, enhancing a type I IFN response via CD40 stimulation in a coordinated fashion with CD47/SIRPα blockade powerfully enhances antitumor immunity. The observation that SIRPα-Fc-CD40L stimulated dose-dependent elevation in multiple serum cytokines and $CD40^+$ B-cell margination in cynomolgus macaques, without causing hemolysis or thrombocytopenia, provides justification to further explore this strategy in human patients with cancer.

Disclosure of Potential Conflicts of Interest

S. de Silva is Vice President, Product Development at Shattuck Labs, Inc. G. Fromm is Vice President, Research and Development at and has ownership interest (including patents) in Shattuck Labs, Inc. C.W Shuptrine is a principal scientist I at Shattuck Labs, Inc. K. Johannes is a research associate at and has ownership interest (including patents) in Shattuck Labs, Inc. K.J. Yoo is a research

associate I at Shattuck Labs, Inc. K. Huang is a research associate II at Shattuck Labs, Inc. T.H. Schreiber is Chief Scientific Officer at and has ownership interest (including patents) in Shattuck Labs, Inc. No potential conflicts of interest were disclosed by the other author.

Authors' Contributions

Conception and design: S. de Silva, G. Fromm, T.H. Schreiber
Development of methodology: S. de Silva, G. Fromm, C.W. Shuptrine, K. Johannes, A. Patel, K. Huang, T.H. Schreiber
Acquisition of data (provided animals, acquired and managed patients, provided facilities, etc.): S. de Silva, G. Fromm, C.W. Shuptrine, K. Johannes, K.J. Yoo, T.H. Schreiber
Analysis and interpretation of data (e.g., statistical analysis, biostatistics, computational analysis): S. de Silva, G. Fromm, C.W. Shuptrine, K. Johannes, K.J. Yoo, K. Huang, T.H. Schreiber
Writing, review, and/or revision of the manuscript: S. de Silva, G. Fromm, T.H. Schreiber
Administrative, technical, or material support (i.e., reporting or organizing data, constructing databases): G. Fromm, K.J. Yoo, T.H. Schreiber
Study supervision: S. de Silva, G. Fromm, T.H. Schreiber

Acknowledgments

This work was supported by Shattuck Labs, Inc.

The costs of publication of this article were defrayed in part by the payment of page charges. This article must therefore be hereby marked *advertisement* in accordance with 18 U.S.C. Section 1734 solely to indicate this fact.

Received July 17, 2019; revised October 16, 2019; accepted December 10, 2019; published first December 18, 2019.

References

1. Feng M, Jiang W, Kim BYS, Zhang CC, Fu YX, Weissman IL. Phagocytosis checkpoints as new targets for cancer immunotherapy. Nat Rev Cancer 2019;19:568–86.
2. Oldenborg PA, Zheleznyak A, Fang YF, Lagenaur CF, Gresham HD, Lindberg FP. Role of CD47 as a marker of self on red blood cells. Science 2000;288:2051–4.
3. Olsson M, Bruhns P, Frazier WA, Ravetch JV, Oldenborg PA. Platelet homeostasis is regulated by platelet expression of CD47 under normal conditions and in passive immune thrombocytopenia. Blood 2005;105:3577–82.
4. Yamao T, Noguchi T, Takeuchi O, Nishiyama U, Morita H, Hagiwara T, et al. Negative regulation of platelet clearance and of the macrophage phagocytic response by the transmembrane glycoprotein SHPS-1. J Biol Chem 2002;277:39833–9.
5. Yi T, Li J, Chen H, Wu J, An J, Xu Y, et al. Splenic dendritic cells survey red blood cells for missing self-CD47 to trigger adaptive immune responses. Immunity 2015;43:764–75.
6. Blazar BR, Lindberg FP, Ingulli E, Panoskaltsis-Mortari A, Oldenborg PA, Iizuka K, et al. CD47 (integrin-associated protein) engagement of dendritic cell and macrophage counterreceptors is required to prevent the clearance of donor lymphohematopoietic cells. J Exp Med 2001;194:541–9.
7. Feng M, Marjon KD, Zhu F, Weissman-Tsukamoto R, Levett A, Sullivan K, et al. Programmed cell removal by calreticulin in tissue homeostasis and cancer. Nat Commun 2018;9:3194.
8. Chao MP, Weissman IL, Majeti R. The CD47-SIRPalpha pathway in cancer immune evasion and potential therapeutic implications. Curr Opin Immunol 2012;24:225–32.
9. Weiskopf K, Ring AM, Schnorr PJ, Volkmer JP, Volkmer AK, Weissman IL, et al. Improving macrophage responses to therapeutic antibodies by molecular engineering of SIRPalpha variants. Oncoimmunology 2013;2:e25773.
10. Willingham SB, Volkmer JP, Gentles AJ, Sahoo D, Dalerba P, Mitra SS, et al. The CD47-signal regulatory protein alpha (SIRPa) interaction is a therapeutic target for human solid tumors. Proc Natl Acad Sci U S A 2012;109:6662–7.
11. Liu X, Pu Y, Cron K, Deng L, Kline J, Frazier WA, et al. CD47 blockade triggers T cell-mediated destruction of immunogenic tumors. Nat Med 2015;21:1209–15.
12. Xu MM, Pu Y, Han D, Shi Y, Cao X, Liang H, et al. Dendritic cells but not macrophages sense tumor mitochondrial DNA for cross-priming through signal regulatory protein alpha signaling. Immunity 2017;47:363–73.
13. Hildner K, Edelson BT, Purtha WE, Diamond M, Matsushita H, Kohyama M, et al. Batf3 deficiency reveals a critical role for CD8alpha+ dendritic cells in cytotoxic T cell immunity. Science 2008;322:1097–100.
14. Bennett SR, Carbone FR, Karamalis F, Flavell RA, Miller JF, Heath WR. Help for cytotoxic-T-cell responses is mediated by CD40 signalling. Nature 1998;393:478–80.
15. Delamarre L, Holcombe H, Mellman I. Presentation of exogenous antigens on major histocompatibility complex (MHC) class I and MHC class II molecules is differentially regulated during dendritic cell maturation. J Exp Med 2003;198:111–22.
16. O'Connell PJ, Morelli AE, Logar AJ, Thomson AW. Phenotypic and functional characterization of mouse hepatic CD8 alpha+ lymphoid-related dendritic cells. J Immunol 2000;165:795–803.
17. Schoenberger SP, Toes RE, van der Voort EI, Offringa R, Melief CJ. T-cell help for cytotoxic T lymphocytes is mediated by CD40-CD40L interactions. Nature 1998;393:480–3.
18. Yasumi T, Katamura K, Yoshioka T, Meguro TA, Nishikomori R, Heike T, et al. Differential requirement for the CD40-CD154 costimulatory pathway during Th cell priming by CD8 alpha+ and CD8 alpha- murine dendritic cell subsets. J Immunol 2004;172:4826–33.
19. Byrne KT, Vonderheide RH. CD40 stimulation obviates innate sensors and drives T cell immunity in cancer. Cell Rep 2016;15:2719–32.
20. Yao X, Wu J, Lin M, Sun W, He X, Gowda C, et al. Increased CD40 expression enhances early STING-mediated type I interferon response and host survival in a rodent malaria model. PLoS Pathog 2016;12:e1005930.
21. Lin GHY, Chai V, Lee V, Dodge K, Truong T, Wong M, et al. TTI-621 (SIRPalphaFc), a CD47-blocking cancer immunotherapeutic, triggers phagocytosis of lymphoma cells by multiple polarized macrophage subsets. PLoS One 2017;12:e0187262.
22. Petrova PS, Viller NN, Wong M, Pang X, Lin GH, Dodge K, et al. TTI-621 (SIRPalphaFc): a CD47-blocking innate immune checkpoint inhibitor with broad antitumor activity and minimal erythrocyte binding. Clin Cancer Res 2017;23:1068–79.
23. Ingram JR, Blomberg OS, Sockolosky JT, Ali L, Schmidt FI, Pishesha N, et al. Localized CD47 blockade enhances immunotherapy for murine melanoma. Proc Natl Acad Sci U S A 2017;114:10184–9.
24. Kornbluth RS, Stempniak M, Stone GW. Design of CD40 agonists and their use in growing B cells for cancer immunotherapy. Int Rev Immunol 2012;31:279–88.
25. Kauder SE, Kuo TC, Harrabi O, Chen A, Sangalang E, Doyle L, et al. ALX148 blocks CD47 and enhances innate and adaptive antitumor immunity with a favorable safety profile. PLoS One 2018;13:e0201832.
26. Vitale LA, Thomas LJ, He LZ, O'Neill T, Widger J, Crocker A, et al. Development of CDX-1140, an agonist CD40 antibody for cancer immunotherapy. Cancer Immunol Immunother 2019;68:233–45.
27. Merz C, Sykora J, Marschall V, Richards DM, Heinonen K, Redondo Muller M, et al. The hexavalent CD40 agonist HERA-CD40L induces T-cell-mediated antitumor immune response through activation of antigen-presenting cells. J Immunother 2018;41:385–98.
28. Vonderheide RH, Flaherty KT, Khalil M, Stumacher MS, Bajor DL, Hutnick NA, et al. Clinical activity and immune modulation in cancer patients treated with CP-870,893, a novel CD40 agonist monoclonal antibody. J Clin Oncol 2007;25:876–83.
29. Fromm G, de Silva S, Johannes K, Patel A, Hornblower JC, Schreiber TH. Agonist redirected checkpoint, PD1-Fc-OX40L, for cancer immunotherapy. J Immunother Cancer 2018;6:149.
30. Rakhmilevich AL, Alderson KL, Sondel PM. T-cell-independent antitumor effects of CD40 ligation. Int Rev Immunol 2012;31:267–78.
31. Lander GC, Stagg SM, Voss NR, Cheng A, Fellmann D, Pulokas J, et al. Appion: an integrated, database-driven pipeline to facilitate EM image processing. J Struct Biol 2009;166:95–102.

32. Sorzano CO, Marabini R, Velazquez-Muriel J, Bilbao-Castro JR, Scheres SH, Carazo JM, et al. XMIPP: a new generation of an open-source image processing package for electron microscopy. J Struct Biol 2004;148:194–204.
33. Oberst MD, Auge C, Morris C, Kentner S, Mulgrew K, McGlinchey K, et al. Potent immune modulation by MEDI6383, an engineered human OX40 ligand IgG4P Fc fusion protein. Mol Cancer Ther 2018;17:1024–38.
34. Gardai SJ, McPhillips KA, Frasch SC, Janssen WJ, Starefeldt A, Murphy-Ullrich JE, et al. Cell-surface calreticulin initiates clearance of viable or apoptotic cells through trans-activation of LRP on the phagocyte. Cell 2005;123:321–34.
35. Chao MP, Alizadeh AA, Tang C, Myklebust JH, Varghese B, Gill S, et al. Anti-CD47 antibody synergizes with rituximab to promote phagocytosis and eradicate non-Hodgkin lymphoma. Cell 2010;142:699–713.
36. Chao MP, Jaiswal S, Weissman-Tsukamoto R, Alizadeh AA, Gentles AJ, Volkmer J, et al. Calreticulin is the dominant pro-phagocytic signal on multiple human cancers and is counterbalanced by CD47. Sci Transl Med 2010;2:63ra94.
37. Katakam AK, Brightbill H, Franci C, Kung C, Nunez V, Jones C III, et al. Dendritic cells require NIK for CD40-dependent cross-priming of CD8+ T cells. Proc Natl Acad Sci U S A 2015;112:14664–9.
38. Lind EF, Ahonen CL, Wasiuk A, Kosaka Y, Becher B, Bennett KA, et al. Dendritic cells require the NF-kappaB2 pathway for cross-presentation of soluble antigens. J Immunol 2008;181:354–63.
39. Valle A, Zuber CE, Defrance T, Djossou O, De Rie M, Banchereau J. Activation of human B lymphocytes through CD40 and interleukin 4. Eur J Immunol 1989;19:1463–7.
40. Cayabyab M, Phillips JH, Lanier LL. CD40 preferentially costimulates activation of CD4+ T lymphocytes. J Immunol 1994;152:1523–31.
41. Kindler V, Matthes T, Jeannin P, Zubler RH. Interleukin-2 secretion by human B lymphocytes occurs as a late event and requires additional stimulation after CD40 cross-linking. Eur J Immunol 1995;25:1239–43.
42. Advani R, Flinn I, Popplewell L, Forero A, Bartlett NL, Ghosh N, et al. CD47 Blockade by Hu5F9-G4 and rituximab in non-Hodgkin's lymphoma. N Engl J Med 2018;379:1711–21.
43. Sikic BI, Lakhani N, Patnaik A, Shah SA, Chandana SR, Rasco D, et al. First-in-human, first-in-class phase I trial of the anti-CD47 antibody Hu5F9-G4 in patients with advanced cancers. J Clin Oncol 2019;37:946–53.
44. Vonderheide RH. The immune revolution: a case for priming, not checkpoint. Cancer Cell 2018;33:563–9.
45. Brierley CK, Staves J, Roberts C, Johnson H, Vyas P, Goodnough LT, et al. The effects of monoclonal anti-CD47 on RBCs, compatibility testing, and transfusion requirements in refractory acute myeloid leukemia. Transfusion 2019;59:2248–54.
46. Liu J, Wang L, Zhao F, Tseng S, Narayanan C, Shura L, et al. Pre-clinical development of a humanized anti-CD47 antibody with anti-cancer therapeutic potential. PLoS One 2015;10:e0137345.
47. Jaiswal S, Jamieson CH, Pang WW, Park CY, Chao MP, Majeti R, et al. CD47 is upregulated on circulating hematopoietic stem cells and leukemia cells to avoid phagocytosis. Cell 2009;138:271–85.
48. Weiskopf K, Ring AM, Ho CC, Volkmer JP, Levin AM, Volkmer AK, et al. Engineered SIRPalpha variants as immunotherapeutic adjuvants to anticancer antibodies. Science 2013;341:88–91.
49. Zhao XW, van Beek EM, Schornagel K, Van der Maaden H, Van Houdt M, Otten MA, et al. CD47-signal regulatory protein-alpha (SIRPalpha) interactions form a barrier for antibody-mediated tumor cell destruction. Proc Natl Acad Sci U S A 2011;108:18342–7.
50. Tseng D, Volkmer JP, Willingham SB, Contreras-Trujillo H, Fathman JW, Fernhoff NB, et al. Anti-CD47 antibody-mediated phagocytosis of cancer by macrophages primes an effective antitumor T-cell response. Proc Natl Acad Sci U S A 2013;110:11103–8.

Published OnlineFirst December 18, 2019; DOI: 10.1158/2326-6066.CIR-19-0493

Cancer Immunology Research

CD40 Enhances Type I Interferon Responses Downstream of CD47 Blockade, Bridging Innate and Adaptive Immunity

Suresh de Silva, George Fromm, Casey W. Shuptrine, et al.

Cancer Immunol Res 2020;8:230-245. Published OnlineFirst December 18, 2019.